

1 **Early Jurassic climate and atmospheric CO<sub>2</sub> concentration in the**  
2 **Sichuan paleobasin, Southwest China**

3  
4 Xianghui Li<sup>1</sup>, Jingyu Wang<sup>1</sup>, Troy Rasbury<sup>2</sup>, Min Zhou<sup>1</sup>, Zhen Wei<sup>1</sup>, Chaokai Zhang<sup>1</sup>

5 <sup>1</sup>State Key Laboratory for Mineral Deposits Research, School of Earth Sciences and Engineering, Nanjing University,  
6 Nanjing 210023 China.

7 <sup>2</sup>Department of Geosciences, Stony Brook University, Stony Brook, NY 11794-2100, USA

8 *Correpondence to:* Xiangui Li ([leeschhui@126.com](mailto:leeschhui@126.com))

9

10 **Abstract:** Climatic oscillations had been developed through the (Early) Jurassic from marine sedimentary archives, but  
11 remain unclear from terrestrial records. This work presents investigation of climate-sensitive sediments and carbon and  
12 oxygen isotope analyses of lacustrine and pedogenic carbonates for the Early Jurassic Ziliujing Formation from the grand  
13 Sichuan paleobasin (GSB), Southwest China. Sedimentary and stable isotope proxies manifest that an overall secular (semi-)  
14 arid climate dominated the GSB during the Early Jurassic except for the Hettangian. This climate pattern is similar to the  
15 arid climate in the Colorado Plateau region, western North America, but distinct from the relatively warm-humid climate in  
16 North China and high latitude in Southern Hemisphere. The estimated atmospheric CO<sub>2</sub> concentration (*p*CO<sub>2</sub>) from carbon  
17 isotopes of pedogenic carbonates shows a range of 980-2610 ppmV (~ 3.5-10 times the pre-industrial value) with a mean of  
18 1660 ppmV. Three phases of *p*CO<sub>2</sub> (the Sinemurian 1500-2000 ppmV, the Pliensbachian 1000-1500 ppmV, and the early  
19 Toarcian 1094-2610 ppmV) and two events of rapid falling *p*CO<sub>2</sub> by ~1000-1300 ppmV are observed, illustrating the *p*CO<sub>2</sub>  
20 perturbation in the Early Jurassic. The perturbation of *p*CO<sub>2</sub> is compatible with seawater temperature and carbon cycle from  
21 the coeval marine sediments, suggesting a positive feedback of climate to *p*CO<sub>2</sub> through the Early Jurassic.

22

## 23 1. Introduction

24 Global paleotemperatures were possibly 5-10°C higher than present during the Jurassic period based on climate modelling  
25 results (e.g., Rees et al., 1999; Sellwood and Valdes, 2008). However, seawater temperature fluctuated by -5 °C to +5 °C, or  
26 even much higher magnitude (e.g., Suan et al., 2008; Littler et al., 2010), based on estimates from the oxygen isotopes of the  
27 belemnite and bivalve fossils (Dera et al., 2011, and references therein). In the Sinemurian–Pliensbachian age, the mean sea  
28 surface temperatures of the North Atlantic were in excess of 28°C (TEX<sub>86</sub>), comparable with similar palaeolatitudes during  
29 the Cretaceous and Early Cenozoic (Robinson et al., 2017); whereas in the late Pliensbachian age, the northern West Tethys  
30 Ocean (e.g., Paris basin, northern Spain basin) was ~12.7°C (e.g., Gómez et al., 2008; Gómez and Goy, 2011; Arabas et al.,  
31 2017), leading to a polar icesheet hypothesis (e.g., Sellwood and Valdes, 2008; Suan et al., 2010; Dera et al., 2011; Gómez et  
32 al., 2015). At ~183 Ma of the early Toarcian oceanic anoxia event (T-OAE), the surface seawater temperature was high to  
33 ~35°C (e.g., Bailey et al., 2003; Korte et al., 2015), and a high temperature (plateau) even continued in the whole Toarcian  
34 (Dera et al., 2011). Examples of seawater temperature transitions between cold and hot show the climate oscillation through  
35 the Early Jurassic.

36 Data from the terrestrial realm also provide important details of environmental and climatic change (e.g., Hesselbo et al.,  
37 2000; Suan et al., 2010; Jenkyns, 2010; Philippe et al., 2017), from which the oscillated climate could be observed and  
38 revealed too. Terrestrial proxies, such as flora (e.g., Riding et al., 2013; Deng et al., 2017; Philippe et al., 2017), vegetation  
39 (Pole, 2009), and geochemistry (e.g., Riding et al., 2013; Kenny, 2015; Tramoy et al., 2016) as well as the *p*CO<sub>2</sub> record (e.g.,  
40 Retallack, 2001a; Beerling and Royer, 2002; McElwain et al., 2005; Berner, 2006; Steinthorsdottir and Vajda, 2015) provide  
41 an emerging record of the Early Jurassic terrestrial climate and environment changes. Correspondingly, the proxy application  
42 of terrestrial sedimentary archives could play a key role in the global Early Jurassic correlation of the marine and terrestrial  
43 climate.

44 Proxies for *p*CO<sub>2</sub> are the important linkage between the marine and terrestrial climatic condition. Studies of the terrestrial  
45 *p*CO<sub>2</sub> record have focused on the Triassic-Jurassic boundary (e.g., Tanner et al., 2001; Cleveland et al., 2008; Schaller et al.,  
46 2011; Steinthorsdottir and Vajda, 2015) and the Toarcian oceanic anoxic event (McElwain et al., 2005), where *p*CO<sub>2</sub>  
47 estimates range 1000 ppm to 4000 ppmV (e.g., Tanner et al., 2001; Cleveland et al., 2008; Schaller et al., 2011). Few  
48 relatively continuous *p*CO<sub>2</sub> records and coupled terrestrial climate changes have been documented for the Early Jurassic.

49 There are several large Triassic-Jurassic terrestrial basins in West China, in which the Sichuan Basin has a relatively  
50 complete and continuous continental sedimentary sequence of the Upper Triassic-Paleogene (e.g., SBGM, 1991, 1997;  
51 Wang et al., 2010). During the Early Jurassic, the Sichuan Basin was in a Boreotropical climate zone based on  
52 climate-sensitive sediments (Fig. 1a. Boucot et al., 2013), or a warm temperate climate is suggested based on clay mineralogy  
53 and phytogeography (e.g., Dera et al., 2009). In this work, we present a field investigation, including lithofacies and paleosol

54 interpretation, and carbon and oxygen isotope analyses of both lacustrine and pedogenic carbonates in Sichuan Basin. New  
55 results allow us to reconstruct the paleoclimate and relatively consecutive  $p\text{CO}_2$  record through the Early Jurassic, for which  
56 we compare to stable isotopes of marine sediments and estimated sea water temperature.

## 57 **2. Geological setting and stratigraphy**

58 Southwest China, including the provinces of Yunnan, Sichuan, Chongqing, and Guizhou, had been the main part of the  
59 upper Yangtze Plate since the Proterozoic, possibly since the Neoproterozoic. With the amalgamation of the Cathaysia and  
60 Yangtze plates, it became the western South China plate or cratonic basin since the Neoproterozoic (Sinian), and continued to  
61 the late Middle Triassic. By the Indosinian orogeny, new foreland basins were formed since the Late Triassic (e.g., He and  
62 Liao, 1985; Li et al., 2003), recording the Mesozoic and Cenozoic evolution of tectonics, environment, and climate in  
63 Southwest China.

64 The Mesozoic Sichuan paleobasin was confined by the Longmenshan thrust belt in the northwest, the Micangshan-Dabashan  
65 arcuate thrust belt in the northeast (Fig. 1b), and the northern hilly topography boundary of the Yunnan-Guizhou plateau in  
66 the south and east. It was mainly developed during the Late Triassic-Jurassic and includes provincial areas of eastern  
67 Sichuan, entire Chongqing, northern Guizhou, western Hubei, and northwestern Hunan. This Triassic-Jurassic Sichuan  
68 foreland basin was much larger than the present Sichuan Basin in the eastern Sichuan province. We estimate the size of  
69 Sichuan paleobasin is roughly 480,000 km<sup>2</sup> based on lithofacies paleogeography (Fig. 1b. Ma et al., 2009; Li and He, 2014),  
70 and suggest naming this the grand Sichuan paleobasin (GSB).

71 The Mesozoic terrestrial sediments accumulated up to ~9 km (Guo et al., 1996) in the GSB; and the Jurassic part can be as  
72 much as 3-3.5 km thick (SBGM, 1991). Two types of Lower Jurassic deposits have been distinguished (Table 1): the  
73 Baitianba Formation (Fm) in the north (~10%) and the Ziliujing Fm (e.g., SBGM, 1991; Wang et al., 2010) in the south  
74 (over 90% of the basin).

75 The Baitianba Fm was deposited unconformably on the Upper Triassic Xujiahe Fm and is overlain conformably by the  
76 Middle Jurassic Xintiangou Fm / Qianfuyan Fm (Table 1). It is mainly composed of grayish shales and sandstones with coal  
77 layers and massive conglomerates. Abundant plant fossils, sporopollens, conchostracans, bivalves, and gastropods indicate it  
78 is of the Early Jurassic (SBGM, 1991, 1997). Sporopollen assemblages of the Hettangian-Sinemurian age were found in the  
79 lower part (Zhang and Meng, 1987) and the Pliensbachian-Toarcian assemblages were reported in the upper part (Wang et  
80 al., 2010).

81 The Ziliujing Fm is composed of variegated and reddish mudrocks (some shales) intercalated with sandstones, siltstones, and  
82 bioclastic limestones as well as dolomitic marlstones / limy dolomites, conformably or unconformably overlying the Xujiahe  
83 Fm or Luqiao Fm and conformably underlying the Xintiangou Fm (SBGM, 1997. Table 1). It has been dated as the Early

84 Jurassic by fossil assemblages of bivalves, ostracods, conchostracans, and plants. Dinosaur fauna can be well correlated to  
85 the Lufeng Fauna in central Yunnan (e.g., Dong, 1984; SBGM, 1991, 1997; Peng, 2009). This formation is subdivided into  
86 five parts in an ascending order: the Qijiang, Zhenzhuchong, Dongyuemiao, Ma'anshan, and Da'anzhai members (SBGM,  
87 1997. Table 1). Of these, the former two are sometimes combined as the Zhenzhuchong Fm (e.g., SBGM, 1991; Wang et al.,  
88 2010).

89 The Da'anzhai Member is characterized by dark gray to black shales and bioclastic limestones with a southward increase of  
90 reddish mudrocks (SBGM, 1991, 1997; Wang et al., 2010), and is regarded the sediment in a grand Sichuan paleolake (e.g.,  
91 Ma et al., 2009; Li and He, 2014). Ostracod assemblages indicate it is the late Early Jurassic (e.g., Wei, 1982; Wang et al.,  
92 2010). A Re–Os isochron age of  $180.3 \pm 3.2$  Ma associated with an organic carbon isotope excursion indicates that the lower  
93 Da'anzhai Member corresponds to the T-OAE (Xu et al., 2017).

94 The Ma'anshan Member is comprised of violet-red mudrocks with a few greyish, greenish thin-bedded fine sandstones and  
95 siltstones, in which floral fossils are common (Li and Meng, 2003). The Dongyuemiao Member consists of greenish and  
96 reddish mudrocks and siltstones with greyish bioclastic limestone and marlstone, of which abundant bivalve and plant fossils  
97 were reported from eastern Sichuan and Chongqing (Li and Meng, 2003; Meng et al., 2003; Wang et al., 2010). The  
98 Zhenzhuchong Member is dominated by violet red mudrocks/shales intercalated with thin-bedded sandstones and / or  
99 siltstones and numerous plant fossils of the Early Jurassic affinity (e.g., Duan and Chen, 1982; Ye et al., 1986). Taken  
100 together, fossil associations suggest that the three members were deposited in the middle-late Early Jurassic. The age  
101 limitation of the overlying Da'anzhai Member and the correlation to the Lufeng dinosaur fauna places these members in the  
102 Sinemurian – Pliensbachian, and the Zhenzhuchong and Dongyuemiao Fms are suggested to be the Sinemurian (Table 1).

103 The Qijiang Member is composed of quartz arenite interbedded/intercalated with dark shales. Coal seams are often seen in  
104 the middle of the Qijiang Member. This member mainly occurs in the central part of the GSB. It is likely the earliest Jurassic,  
105 possibly Hettangian age, but plant fossils cannot precisely indicate the age (Wang et al., 2010).

### 106 **3. Materials and methods**

107 We have measured sections and made detailed observations and descriptions of sedimentary characteristics for lithofacies  
108 analysis at six outcrop sections (Locations A1 to A4, A6 and A7, Fig. 1). Published descriptions for other sections  
109 (Locations A5, A8, and A9, Fig. 1) are integrated into our observations. Details of microscopic examination of sedimentary  
110 rocks and analysis of sedimentary facies underpinning the climate analysis are attached as the supplementary data Note S1.  
111 Below we state climate-sensitive sediment observation, carbon and oxygen isotope analyses, and estimate of  $p\text{CO}_2$ .

#### 112 **3.1. Observation of climate-sensitive sediments**

113 Climate-sensitive sediments are mainly dolomites, gypsum, and paleosols, which are used to analyze the climate in this work

114 (Table S1).

115 Dolomites and gypsum are relatively easy to recognize in both field and under microscope. We distinguish dolomites from  
116 limestones following Tucker (2011) and Flügel (2004). As Flügel (2004) stated, field distinctions of limestone and dolomite  
117 can also be made although detailed differentiation of carbonate rocks is best performed in the laboratory. In field, we  
118 recognize gypsum by particular structures such as chicken-wire cage, gypsum pseudomorph, and cluster of (0.5-1 cm) pore.  
119 There are multiple classifications of paleosols (e.g., Wright, 1992; Mack et al., 1993; Retallack, 2001b; Imbellone, 2011),  
120 mostly based on the US Soil Taxonomy. We recognized paleosols in the field based on color, structures, horizonation, root  
121 traces, and textures, and followed the general classification paleosols by Mack et al. (1993) and Retallack (2001b). In this  
122 paper, paleosols are described following the procedures of the Soil Survey Manual and classified according to Soil Survey  
123 Staff (1998).

124 Within the measured and observed sections, paleosol profiles were mainly identified from the two main locations/sections  
125 A4 and A6 (Figs. S1 and S2, and Table S2). Horizonation, BK horizon thickness, boundaries, structures, trace fossils,  
126 rootlets, carbonate accumulations (calcretes), etc. were recorded (Table S2). Paleosols interpreted in other cited sections (Fig.  
127 1) rely on the description of lithology, structure, and calcrete in the original references. Based upon a modification of the  
128 Retallack (1998) categorization of paleosol maturity, the relative paleosol development (maturity) was assigned.

### 129 **3.2. Analyses of carbon and oxygen isotopes**

130 Ten lacustrine carbonate samples were analysed for carbon and oxygen isotopes from the Da'anzhai Member at the Shaping  
131 section, Ya'an (Location A4, Fig. S1 and Table S3). 26 pedogenic carbonate samples were analyzed for carbon and oxygen  
132 isotopes from 32 paleosols of the Ziliujing Fm at the same section (Fig. S1 and Table S4). Two or three microdrilling  
133 powder samples (columns 7 and 8 in Table S4) were taken from the same individual calcrete for stable isotope analysis, and  
134 then a mean value for each calcrete sample was calculated (columns 9 and 10 in Table S4).

135 At the field scale, calcretes are ginger-like and sporadically spaced within the soil horizon. We observed no linear and planar  
136 calcretes that would indicate precipitation at or below the water table. Before drilling, thin-sections were petrographically  
137 studied using polarized light microscopy and cathodoluminescence imaging. Micritic calcite is predominant in both  
138 lacustrine and pedogenic carbonate samples, with no evidence for carbonate detritus in calcretes (Fig. 2a and 2b). The  
139 micritic calcites used for stable isotope analyses are chiefly null- to non-luminescent, with <10% light orange and brownish  
140 luminescence, indicating genesis primarily in the vadose zone. While luminescent calcretes indicate a high possibility of  
141 hydrological influence (e.g., Mintz, et al., 2016), we sampled to avoid this. Based on petrography and CL imaging together  
142 with the field observations, the dense micritic zones sampled for the stable isotope composition should give pristine  $\delta^{13}\text{C}$   
143 values that can be used to estimate  $p\text{CO}_2$ .

144 Microsampling of lacustrine and pedogenic carbonates focused on only micrites, avoiding diagenetic spar from cracks, veins,

145 and vug spaces. Powder samples were obtained using a dental drill (aiguille diameter  $\phi=1-2$  mm).  
146 Isotopic analyses were conducted on 0.3 ~ 0.5 mg powder samples. Powder samples were dried in an oven at 60°C for 10  
147 hours before being moved to the instrument. Carbon dioxide for isotopic analysis was released using orthophosphoric acid at  
148 70°C and analysed on-line in a DELTA-Plus xp (CF-IRMS) mass spectrometer at the State Key Laboratory for Mineral  
149 Deposits Research, Nanjing University. The precision of the measurements was regularly checked with a Chinese national  
150 carbonate standard (GBW04405) and the international standard (NBS19) and the standard deviation of  $\delta^{13}\text{C}$  was  $\pm 0.1\%$  over  
151 the period of analysis. Calibration to the international PeeDee Belemnite (PDB) scale was performed using NBS19 and  
152 NBS18 standards.

### 153 3.3. Calculation of atmospheric CO<sub>2</sub> concentration

154 The Cerling (1991, 1999) equation was used to calculate the  $p\text{CO}_2$  using the carbon isotope of pedogenic carbonates as  
155 below:

$$156 C_a = S_{(z)}(\delta^{13}\text{C}_s - 1.0044\delta^{13}\text{C}_r - 4.4)/(\delta^{13}\text{C}_a - \delta^{13}\text{C}_s)$$

157 where  $C_a$  is  $p\text{CO}_2$ ;  $\delta^{13}\text{C}_s$ ,  $\delta^{13}\text{C}_r$ ,  $\delta^{13}\text{C}_a$  are the isotopic compositions (‰) of soil CO<sub>2</sub>, soil-respired CO<sub>2</sub>, and atmospheric CO<sub>2</sub>,  
158 respectively; and  $S_{(z)}$  is the CO<sub>2</sub> contributed by soil respiration (ppmV).

159  $\delta^{13}\text{C}_s$  is often calibrated by fractionation factor  $-8.98\%$  with the formula  $-8.98\% + \delta^{13}\text{C}_c$  (Ekart et al., 1999), with which  $\delta^{13}\text{C}_c$   
160 is the measured result of pedogenic calcrite. Alternatively,  $\delta^{13}\text{C}_s$  can be replaced by  $\delta^{13}\text{C}_{sc}$ , which is calibrated by carbon  
161 isotope ratio of pedogenic carbonate at 25°C based on latitude–temperature correlations (Besse and Courtillot, 1988; Ekart et  
162 al., 1999) following the equation  $\delta^{13}\text{C}_{sc} = (\delta^{13}\text{C}_c + 1000)/((11.98 - 0.12 * T)/1000 + 1) - 1000$  (Romanek et al., 1992). We used  
163 both  $\delta^{13}\text{C}_s$  and  $\delta^{13}\text{C}_{sc}$  to calculate the  $p\text{CO}_2$  (Table S4).

164  $\delta^{13}\text{C}_r$  represents carbon isotope ratio of average bulk C3 vascular tissue (Arens et al., 2000), reflecting atmospheric  $\delta^{13}\text{C}$   
165 (Jahren et al., 2008). The  $\delta^{13}\text{C}_{om}$  of organic matter within paleosols based on the range of modern C3 ecosystem  
166 fractionations (Buchmann, et al., 1998; Ekart et al., 1999), is commonly used for  $\delta^{13}\text{C}_r$ . However, the  $\delta^{13}\text{C}_r$  could be  
167 compromised in fossil soils due to oxidation and metabolism of organic matter after burial (Nadelhofer and Fry, 1988). In  
168 this paper, we use the  $\delta^{13}\text{C}_{om}$  from the Paris Basin (Bougeault et al., 2017; Peti et al., 2017) for the Sinemurian-Pliensbachian  
169  $\delta^{13}\text{C}_r$  and from Cardigan Bay, UK (Xu et al., 2018) for the Toarcian.

170  $\delta^{13}\text{C}_a$ , the carbon isotopic composition of the atmosphere, was about  $-8\%$  in the 1980s, being depleted relative to the  
171 pre-industrial atmosphere which was around  $-6.5\%$  (Friedli et al., 1986). The average value of  $-6.5\%$  has been chosen as the  
172  $\delta^{13}\text{C}_a$  for acquiring  $\delta^{13}\text{C}_r$  and  $S_{(z)}$  (e.g., Ekart et al., 1999; Robinson et al., 2002), and the  $\delta^{13}\text{C}_a$  was generally calibrated as  
173  $\delta^{13}\text{C}_{ac}$  from  $\delta^{13}\text{C}_r$  using the formula  $(\delta^{13}\text{C}_r + 18.67)/1.1$  (Arens et al., 2000). Herein we used both calibrations to calculate the  
174  $\delta^{13}\text{C}_a$  (Table S4).

175  $S_{(z)}$  is the largest source of uncertainty in  $p\text{CO}_2$  estimates (Breecker, 2013) and the uncertainty arises primarily from their  
176 sensitivity to soil-respired  $\text{CO}_2$  ( $S_{(z)}$ ) (Montañez, 2013). It is a function of depth and effectively constant below 50 cm (e.g.,  
177 Cerling, 1991).  $S_{(z)}=2500$  ppmV is suggested for the sub-humid temperate and tropical climates (Breecker et al., 2010),  
178 2500-5000 ppmV for higher moisture and productivity soil (Montañez, 2013), 2000 ppmV for semi-arid areas (Breecker et  
179 al., 2009), 1500-2000 ppmV for aridisols and alfisols (calcisol-argillisol) and  $2000\pm 1000$  for paleo-vertisol (Montañez,  
180 2013), and 1000 ppmV in desert areas (Breecker et al., 2010) or  $400 \pm 200$  ppmV for immature soil (Montañez, 2013). In  
181 this context, we chose the  $S_{(z)}=2000$  ppmV for calculating  $p\text{CO}_2$  at  $25^\circ\text{C}$  as the calcisols are reddish-brownish aridisols, and  
182 we also compared the results with that by  $S_{(z)}=2500$  ppmV (Table S4). Additionally, we took samples at the middle and  
183 lower Bk horizon (often  $> \sim 20\text{-}30$  cm to the BK top). That means the depth of calcrete samples in the examined palaeosols  
184 was generally deeper than 50 cm below the paleosol surface, meeting the requirement for a constant value of  $S_{(z)}$ .

## 185 **4. Results**

186 Based on the investigation of cross-sections (locations A1-A4, and A6-A7. Fig. 1), we have classified six sedimentary facies  
187 units in the Ziliujing Fm. They are alluvial fan, fluvial river, flood plain, lake, lake-delta, and swamp facies. Details of  
188 description and interpretation are in the supplementary data Note S1. Below are results of climate-sensitive sediment  
189 observation, stable isotope analyses, and  $p\text{CO}_2$  calculation.

### 190 **4.1. Climate-sensitive sediments**

191 Field observation combined with published calcrete materials shows that paleosols widely occur in the Lower Jurassic  
192 Ziliujing Fm of the GSB (Figs. 1, 3, and 4). A total of 32 paleosols were observed and described at the Shaping section,  
193 Ya'an, and five paleosols were found at the Tanba section, Hechuan (Table S2).

194 Most of paleosols are reddish (GSA Munsell Rock-Color 5R 2/2, 5R 3/4, 5R 4/2) and brownish (10R 3/4, 10R 5/4) (Fig. 3  
195 and Table S2). Peds of paleosols are mainly angular and subangular, and a few are prismatic and platy. Slickensides are  
196 common. Mottles (Fig. 3a), rootlets /rhizoliths (Fig. 3c), and burrows sometimes occur with strong leaching structures (Fig.  
197 3a). Occasionally mudcracks are associated with the aforementioned structures (Fig. 3d).

198 All paleosols are calcic with more or less calcretes in Bk horizons. The thickness of Bk horizons mainly changes from 30 cm  
199 and 100 cm, and partly up to 170 cm (Table S2). Calcretes are generally ginger-like, ellipsoid, subglobular, and irregular in  
200 shape (Fig. 3b and 3e) and nodules are 1-3 cm even up to 8-15 cm (paleosols J1z-10-01 and J1z-12-01) in size (Fig. 3e).  
201 Calcrete is often less than 0.5-1% in an individual paleosol, but a few can be up to 3-5% (paleosol J1z-3-01. Fig. 3b) even 10%  
202 (paleosols J1z-5-02 and 18HC-10).

203 All above paleosols are defined as relatively mature calcisols (Mack et al., 1993), a kind of aridisol (Soil Survey Staff, 1998;  
204 Retallack, 2001b). The original lithofacies were chiefly argillaceous and silty (split-fan) overbank, interchannel, and flood



205 plain deposits (Figs. S1 and S2). Some formed landward the paleo-lakeshore.  
206 Dolomites were found at seven loactions in central and southern GSB (Figs. 1, 4, and Table S1). The dolomites chiefly occur  
207 in the Toracian Da'anzhai Member and a few in the Sinemurian-Plienbachian Dongyuemiao and Ma'anshan members (Fig.  
208 4). They are often massive whitish (Figs. 3f and S3e) and micritic (Figs. S4b and S4d), likely indicating an authigenic origin.  
209 Gypsum is recorded in two loactions (Figs. 1, 4, and Table S1). One is located at Zigong (Location A5. SBG, 1980a). The  
210 other lies at Hechuan (Location A6), which can be identified by chicken-wire cage structure and is associated with micriditic  
211 dolomites (Fig. 3f).

## 212 4.2. Carbon and oxygen isotope values

213  $\delta^{13}\text{C}$  values of lacustrine carbonate samples range from -2.02‰ to -4.07‰ and  $\delta^{18}\text{O}$  values range from -9.91‰ to -12.28‰  
214 (Table S3 and Fig. 5). An increasing trend of both carbon and oxygen isotope ratios is observed from lower to upper  
215 horizons across a 45 m stratal interval of the lower Da'anzhai Member (Fig. 6).

216 Pedogenic carbonate samples have  $\delta^{13}\text{C}$  values from -3.52‰ to -8.10‰, which fall in the typical stable isotope range for  
217 pedogenic carbonates. Values of -6‰ to -8.0‰ characterize the sequence of the Zhenzhuchong Member and main  
218 Ma'anshan Member, with an abrupt increase to -5.5‰ to -3.5‰ at the top of Ma'anshan Member (samples J1z-16-01 and  
219 J1z-18-01. Fig. 6).  $\delta^{18}\text{O}$  values are mainly from -11.3‰ to -13.10‰ in the interval of the Zhenzhuchong Member and  
220 Ma'anshan Member.  $\delta^{18}\text{O}$  follows  $\delta^{13}\text{C}$  with a sudden increase to -5.5‰ at the top of the Ma'anshan Member (Fig. 6). Large  
221 and frequent variations of both carbon and oxygen isotope ratios can be observed in the lower Da'anzhai Member (Fig. 6 and  
222 Table S4).

## 223 4.3. CO<sub>2</sub> concentrations

224  $p\text{CO}_2$  values based on paleobarometer modelling of paleosol calcite (Cerling, 1999) vary depending on the parameters used  
225 for the calculation.

226 If  $S_{(z)}=2500$  ppmV and  $\delta^{13}\text{C}_a=-6.5$ ‰ (constant pre-industrial atmosphere),  $p\text{CO}_2$  values range between ~1140 ppmV and  
227 ~3460 ppmV with a mean of 1870 ppmV (column 15 in Table S4); and when  $S_{(z)}=2500$  ppmV and  $\delta^{13}\text{C}_a=(\delta^{13}\text{C}_r+18.67)/1.1$ ,  
228  $p\text{CO}_2$  values change between ~1230 ppmV and ~3260 ppmV with a mean of 2070 ppmV (column 16 in Table S4).

229 When  $S_{(z)}=2000$  ppmV and  $\delta^{13}\text{C}_s=-8.98+\delta^{13}\text{C}_c$  are used,  $p\text{CO}_2$  values are ~ 940-2530 ppmV with the mean 1600 ppmV  
230 (column 17 in Table S4); and if  $S_{(z)}=2000$  ppmV and  $\delta^{13}\text{C}_s=(\delta^{13}\text{C}_c+1000)/((11.98-0.12*25)/1000+1)-1000$  are adopted,  
231  $p\text{CO}_2$  values become ~980 ppmV to ~2610 ppmV with the mean 1660 ppmV (column 18 in Table S4). Details of the  
232 different parameters and  $p\text{CO}_2$  results can be seen in Table S4.

233 Results further show that  $p\text{CO}_2$  values at  $S_{(z)}=2500$  ppmV are larger than at  $S_{(z)}=2000$  ppmV. The highest difference is ~  
234 1000 (3640-2610) ppmV, while the lowest is ~300 (1230-930) ppmV and the mean is ~ 370 (2070-1600) ppmV. In addition,

235 when  $S_{(z)}$  is the same, the  $p\text{CO}_2$  values are close even if other parameters are different (comp. between columns 15 and 16,  
236 17 and 18 in Table S4, and Fig. 6).

237 Whatever parameters used, the trend of  $p\text{CO}_2$  over the epoch is quite similar (Fig. 6). We chose  $S_{(z)}=2000$  ppmV (column 18  
238 in Table S4) to illustrate the nature of the Early Jurassic  $p\text{CO}_2$  in the GSB.

239  $p\text{CO}_2$  values mostly range between 980 ppmV and 2610 ppmV, and the mean 1660 ppmV is  $\sim 6$  times the pre-industrial 275  
240 ppmV. Most of the  $p\text{CO}_2$  values are 1000-2000 ppmV with the mean 1580 ppmV in the Zhenzhuchong and Ma'anshan  
241 members,  $\sim 3.5$ - $7.5$  times the pre-industrial  $p\text{CO}_2$  value.

242 It is noted that the errors of  $p\text{CO}_2$  range from 384 ppmV to 1017 ppmV with a mean 647 ppmV (Table S5), leading to a large  
243 uncertainty of the mean  $\sim 39\%$ . The largest source of the uncertainty is the standard error (766 ppmV) of modern soil carbonate  
244 (Breecker and Retallack, 2014). The  $p\text{CO}_2$  uncertainty decreases by  $\sim 20\%$  if half (383 ppmv) of the standard error of soil  
245 carbonate is selected, and decreases to  $\sim 12\%$  if 1/4 ( $\sim 191$  ppmV) standard error is used. The second largest source of error in  
246 the  $p\text{CO}_2$  is the  $S_{(z)}$  estimate. The uncertainty of  $p\text{CO}_2$  becomes much smaller when the  $S_{(z)}$  is larger, e.g., it will fall from  $\sim 39\%$   
247 to  $\sim 17\%$  if  $S_{(z)}=5000$  ppmV instead of 2000 ppmV. Other parameters such as temperature,  $\delta^{13}\text{C}_r$ ,  $\delta^{13}\text{C}_a$ ,  $\delta^{13}\text{C}_s$ , contribute very  
248 little to the calculated  $p\text{CO}_2$  uncertainty. The uncertainty of  $p\text{CO}_2$  is same when either  $\delta^{13}\text{C}_a$  is determined by the transfer from  
249  $\delta^{13}\text{C}_c$  of marine planktonic fossil carbonates (Table S8) or organic matters (Table S5).

## 250 **5. Discussion**

251 The Jurassic marine record shows climatic and environmental oscillations (e.g., van de Schootbrugge et al., 2005; Dera et al.,  
252 2011; Gómez et al., 2015; Arabas et al., 2017), including sea water temperature fluctuation and carbon cycle reorganization  
253 recorded in both carbonate and organic matter. The climate changes and events recorded in the the marine realm have been  
254 mainly attributed to Karoo-Ferrar volcanism (e.g., Hesselbo et al., 2000; Caruthers et a., 2013), sea-level change (e.g.,  
255 Hesselbo and Jenkyns, 1998; Hallam and Wignall, 1999), orbital forcing (e.g., Kemp et al., 2005; Huang and Hesselbo, 2014,  
256 Storm et al., 2020), and / or the opening of the Hispanic corridor (e.g., van de Schootbrugge et al., 2005; Arias, 2009).  
257 Eruption of the Karoo-Ferrar and Central Atlantic mgama is thought to have released large amounts of  $\text{CO}_2$  into the  
258 atmosphere in a short amount of time, resulting in rising temperatures of both marine and continental realms. The nearly  
259 continuous record of Jurassic strata in the GSB provides an excellent test of this hypothesis in the terrestrial realm. We  
260 compare the climate and  $p\text{CO}_2$  record from the GSB in relationship to the marine temperature records.

### 261 **5.1. Paleoclimate variation**

262 During the Late Triassic, Southwest China was warm-hot and humid and occupied a tropical and / or subtropical zone, as  
263 demonstrated by palynoflora, coals, and perennial riverine and lacustrine lithofacies in the Xujiahe Fm (e.g., Huang, 1995; Li  
264 et al., 2016). However, the climate became dry through the Early Jurassic manifested by climate-sensitive sediments and

265 stable isotopes albeit there are two lithofacies packages reflecting two major lake stages (for details refer to supplementary  
266 data Note S1) in the GSB.

### 267 **5.1.1 The Hettangian Age**

268 In the Hettangian, the climate was warm-humid like the Late Triassic in the GSB. The Qijiang Member is comprised of  
269 mainly mature quartz arenites and siltstones with coals (Fig. 7) as well as siderite concretions, indicating a stable tectonic  
270 setting and warm-humid climate in the eastern and southern GSB. Climate was similar across the whole region, because  
271 multiple coal layers occur in the lower Baitianba Fm. The alluvial fan system of the lower Baitianba Fm. (Figs. 7 and S6) is  
272 characterized by moderate-good roundness and sorting of gravels with sandy matrix (Fig. S3a. e.g., Liu et al., 2016; Qian et  
273 al., 2016; and this work). In the Newark basin of eastern North America, climate-sensitive sediments such as nodules of  
274 carbonate and gypsum (pseudomorph) as well as mudcrack in mudflat facies indicate an arid climate in the fifth cycle of the  
275 Hettangian (>199 Ma) Passaic Fm (Kent et al., 2017). More widespread, the eolian Navajo Sandstone, dated as  
276 Hettangian-Sinemurian (200-195 Ma. Parrish et al., 2019), indicates arid in Colorado Plateau (Fig. 1a. Boucot et al., 2013).

### 277 **5.1.2 The Sinemurian Age**

278 The early Sinemurian Zhenzhuchong Member is a combination of riverine flood plain and lacustrine facies (supplementary  
279 Note S1). The lithology is dominated by violet-red mudrocks with few thin greyish, greenish fine sandstones and siltstones.  
280 The reddish color of rocks may indicate a change of climate. Differences in the color appearance show that the reddish color  
281 started in the middle member in the central basin (Location A6. Fig. S2) but almost developed through the whole member in  
282 the western basin (Location A4. Fig. 6).

283 Within reddish mudrocks of the flood plain facies, multiple calcisols were observed at the Shaping section, Ya'an (Location  
284 A4. Figs. 1, 4, and 7), including a strongly leached calcisol horizon (Fig. S3c). We also interpret the reddish muddy  
285 sediments with abundant calcretes as the calcisol at sections of Dafang (Location A8. Zhang et al., 2016), Tianzhu (Location  
286 A9. Li and Chen, 2010), and Weiyuan (Location A10. SBG, 1980a). The calcisols indicate a (semi-) arid climate in the  
287 Sinemurian.

288 This climate change, interpreted from reddish mudrocks and paleosols, is consistent with the floral fossils (e.g., Huang, 2001;  
289 Wang et al., 2010), suggesting the decreasing humidity and increasing temperature from the Late Triassic epoch and the  
290 Hettangian age into the Sinemurian age in the southern GSB. However, in the northern GSB there are few proxies for  
291 climate change, and alluvial fan and lacustrine delta facies common in the middle Baitianba Fm (Fig. S6. e.g., Qian et al.,  
292 2016) do not give us information on climate.

293 The late Sinemurian Dongyuemiao Member also has reddish mudrocks and calcisols, similar to the Zhenzhuchong Member.  
294 Pedogenic calcretes were reported at Dafang (Location A8. Zhang et al., 2016), Tianzhu (Location A9. Li and Chen, 2010),

295 and Yunyang (Location A15. Meng et al., 2005) and in the central and southern GSB (Figs 4 and 7 and Table S2), indicating  
296 continued arid climate conditions at the time.

297 The interpreted Sinemurian (semi-) arid climate from reddish mudrocks and calcisols is supported by the flora (Li and Meng,  
298 2003) and the mudrock geochemistry (Guo et al., 2017). Few records of coeval terrestrial climate are known from other  
299 continents or regions in the literature. The Whitmore Point Member of the Moenave Fm deposited in dryland lakes (Tanner  
300 and Lucas, 2008) and the upper part of eolian Navajo Sandstone (Blakey et al., 1988) could represent the coevally similar  
301 climate in Colorado Plateau although relatively cool (~9 to 18 °C) continental climate was inferred from oxygen and  
302 hydrogen isotope composition of chert precipitated in interdune, freshwater lakes in the Navajo Sandstone (Kenny, 2015).  
303 With a difference, in eastern England, the co-occurrence of the acmes of thermophilic pollens *Classopollis classoides* and  
304 *Liasidium variabile* indicates the warm-humid climate in the late Sinemurian (Riding et al., 2013).

### 305 **5.1.3 The Pliensbachian Age**

306 The Ma'anshan Member of the Pliensbachian displays a prominent change in the distribution and extent of red color  
307 sediment and pedogenesis. The reddish sediments extend through the entire member (comp. Figs. 6 and S2) and can be  
308 observed across most of the GSB. Calcisols are documented in both the western and central GSB (Figs. 6, 7, S1, and S2).  
309 Ten calcisol horizons were recognized at the Shaping section, Ya'an (Figs. 6 and S1). Strongly leached pedogenic structures  
310 and mudcracks are seen in Bed H8 of the Tanba section, Hechuan (Fig. 3a and 3d). Abundant calcretes within terrestrial red  
311 mudrocks are widely described at Gaoxian of Dafang (Location A8. Zhang et al., 2016), Hulukou of Weiyuan (Location A10.  
312 SBG, 1980a), Geyaoguan of Gulin (Location A13. SBG, 1976), Taiyuan of Fengdu (Location A16. SBG, 1975), and Yaxi of  
313 Zunyi (Location A17. Yang, 2015). The widespread distribution of redbeds and calcisols (Figs. 4 and 7) denotes an  
314 intensification of the (semi-) arid climate.

315 Plant and sporopollen fossils also show a change to drier climate in the Pliensbachian. Compared to the Sinemurian members,  
316 more plant fossils are reported in this member (e.g., Meng and Chen, 1997; Wang et al, 2010). The Pliensbachian-Toarcian  
317 sporopollen assemblages are dominated by sporomorph genera assemblage *Dictyophyllidites-Cyathidites-Classopollis*, in  
318 which the dry-type gymnosperm spore *Classopollis* is more prevalent than in the Hettangian-Sinemurian (Zhang and Meng,  
319 1987).

320 Similar dry temperate / subtropical climate is interpreted for the upland coniferous forest in Qaidam Basin, Northwest China  
321 (Wang et al., 2005) and by interdune playa mudstones of the Kayenta Fm in Colorado Plateau (e.g., Bromley, 1992) albeit it  
322 was a cool-humid climate in South Kazakhstan, central Asia (Tramoy et al., 2016).

### 323 **5.1.4 The Toarcian Age**

324 In spite the fact that the Da'anzhai Member was deposited in the largest lacustrine transgression period (Fig. 7. details see

325 supplementary data Note S1), abundant evidence for arid conditions, including backshore reddish mudrocks with calcisols,  
326 lacustrine micritic dolomites and / or gypsum, and stable isotopic geochemistry of lacustrine carbonate, indicate that the  
327 Toarcian aridification could be the most intensive of the late Early Jurassic in the GSB.

328 Redbeds with abundant calcretes are well developed in this member (Figs. 4 and 7). Four calcisols in the Shaping section  
329 (Figs. 6 and S1) and the leaching/illuvial structure (Bed H13) in the Tanba section (Fig. 3c) were observed. Calcisols with  
330 calcretes also occur at sections of Dafang (Location A8. Zhang et al., 2016), Nanxi (Location A11. SBG 1980a), Gongxian  
331 (Location A12. Liang et al., 2006), and Yunyang (Location A15. Meng et al., 2005). The widespread occurrence of calcisols  
332 within the lacustrine facies reveals that subaerial exposure of sediments often interrupted the lake environment, illustrating  
333 dynamic lake level fluctuations and an arid climate.

334 Gypsum and micritic dolomites are reported in the western and southern GSB (SBG, 1980a; Mo and Yu, 1987; Peng, 2009;  
335 and this work) (Figs. 1, 4, and 7). Though there are a number of hypotheses on the dolomite formation in deep time, such as  
336 authigenic origin, diagenetic replacement, microbial mediation (e.g., Vasconcelos et al., 1995; Mckenzie et al., 2009; Petrash  
337 et al., 2017), a high abundance of dolomite was interpreted to form during greenhouse periods, characterized by warm  
338 climates, probably reflecting favourable conditions for evaporite deposition and dolomitization via hypersaline reflux  
339 (Warren, 2000). Dolomites are also thought the results of interplay of climate and sea-level / base-level change (e.g.,  
340 Newport et al., 2017) or are interacted with climatic regimes (Vandeginste et al., 2012). The widespread micritic dolomites  
341 in the Da'anzhai Member, which are associated with gypsum (Fig. 3f), likely indicate an arid climate in the central and  
342 western GSB (Fig. 1b). Gypsum occasionally occurs at Maliuping of Hechuan (Fig. 3f) and Wujiaba of Zigong (SBG,  
343 1980a), showing a possible evaporitic climate in the early Toarcian in the central GSB.

344 Carbon and oxygen isotopes of lacustrine carbonates further support the interpretation of an arid climate in the Toarcian age  
345 in the GSB. The mainly positive  $\delta^{13}\text{C}$  values 0 to 2 ‰ (Fig. 5) from Hechuan (Wang et al., 2006) indicate the lakes were  
346 brackish or even saline. The relatively heavy negative  $\delta^{13}\text{C}$  values -1‰ to -3.5 ‰ (Fig. 5) from Zigong (Wang et al. 2006)  
347 and Ya'an (this work) denote low depletions of  $^{13}\text{C}$  during calcite/aragonite precipitation and mean that the lakes were  
348 possibly brackish. Lightly negative  $\delta^{18}\text{O}$  values -5‰ to -12 ‰ (Fig. 5) of the lacustrine carbonates, suggest closed lacustrine,  
349 palustrine and pond systems formed in a regional arid-semiarid climate with evaporation exceeding precipitation.

350 The covariance of  $\delta^{13}\text{C}$  and  $\delta^{18}\text{O}$  is a criterion to distinguish closed or open lakes (e.g., Talbot, 1990; Li and Ku, 1997).  
351 Pronounced positive covariances ( $R^2=0.44-0.96$ ) between carbon and oxygen isotopes (Fig. 5) indicate a typical  
352 arid-semiarid pattern of lakes in the central and western GSB.

353 The Da'anzhai Member has the same palynofloral assemblage with the Ma'anshan Member, in which the dry-type  
354 gymnosperm spore *Classopollis* is more abundant than in underlying strata (e.g., Zhang and Meng, 1987; Wang et al., 2010),  
355 supporting the aridification indicated by climate-sensitive sediments and stable isotope ratios of lacustrine carbonates  
356 aforementioned.

357 Coastal Cheirolepidiacean (gymnosperm) forests indicate (temperate to subtropical) warm-humid climate punctuated by  
358 locally dry and/or arid events in the Toarcian in Qaidam Basin, Northwest China (Wang et al., 2005). In Inner Mongolia of  
359 North China, the thermophilous plants such as the dipteridaceous fern *Hausmannia*, bennettitales *Ptilophyllum*, display  
360 similar warm and humid climate interrupted by hot and even arid conditions in a short intervals of the Toarcian (Deng et al.,  
361 2017). The warm-wet climate was also indicated by assemblages of sporomorph and vegetation in the late Early Jurassic in  
362 Jurong of Jiangsu, Lower Yangtze area (Huang et al., 2000). In South Kazakhstan, central Asia, paleoflora and  $\delta^2\text{H}$  values  
363 suggest slightly less humid and warmer conditions starting from the early Toarcian (Tramoy et al., 2016).

364 Climate-sensitive sediments, carbon and oxygen isotope values and covariance, and palynoflora, together indicate that an  
365 overall (semi-) arid climate dominated the GSB during the Early Jurassic, possibly accompanied by occasional evaporitic  
366 climate. Relatively abundant calcisols suggest that the GSB was in a subtropical arid zone based on the paleoclimatic  
367 zonation model of paleosols (Mack and James, 1994) during the middle-late Early Jurassic. Through the Early Jurassic, this  
368 (semi-) arid climate in GSB is thoroughly comparable with the simultaneous arid climate recorded in dryland lacustrine and  
369 eolian facies in Colorado Plateau (e.g., Blakey et al., 1988; Bromley, 1992; Tanner and Lucas, 2008; Parrish et al., 2017), but  
370 distinct from the relatively warm-humid climate indicated by sedimentological and floral characteristics in North China (e.g.,  
371 Wang et al., 2005, Deng et al., 2017) and in the relatively high latitudes of Southern Hemisphere (Pole, 2009).

372 In summary, the increasing aridity and warming in the GSB and arid climate in the Colorado Plateau could have been  
373 consecutive through the Early Jurassic, and seems not harmonized with the global fluctuated climate that could be  
374 imprinted by two large volcanic eruptions of the Central Atlantic magmatic province and Karro-Ferrar Large Igneous  
375 Province. The secular arid climate in the two areas might be more possibly constrained by paleotopography, where both were  
376 laid in the relatively low latitudes 15-30°N (Fig. 1a).

## 377 **5.2. $p\text{CO}_2$ perturbations and events**

378 Pedogenic carbonates found in various continental settings precipitate in direct contact with soil atmosphere and bed rock  
379 and hold a meaningful signature of past climate (Alonso-Zarza and Tanner, 2006). There are few high age resolution  $p\text{CO}_2$   
380 reconstructions for the Early Jurassic. The focus on  $p\text{CO}_2$  estimates has on the event horizons, such as the transition of the  
381 Triassic to Jurassic (e.g., Tanner et al., 2001; Schaller et al., 2011). Herein we present a  $p\text{CO}_2$  estimate based on data from  
382 the GSB at ~1.0 Myr age resolution for ~20 Myr (199-179 Ma) interval of the Early Jurassic (Figs. 6 and 8a).

### 383 **5.2.1. $p\text{CO}_2$ perturbation**

384 Results of model estimates show that the  $p\text{CO}_2$  values range 980-2610 ppmV with a mean 1660 ppmV in the Early Jurassic  
385 post the Hettangian and can be divided into three intervals (Figs. 6 and 8a): phase I, stable 1500-2000 (mean ~1700) ppmV  
386 in the Zhenzhuchong and Dongyuemiao members (Sinemurian age); phase II, main 1000-1500 (mean ~ 1300) ppmV in the

387 Ma'anshan Member (Pliensbachian age); and phase III, great fluctuation 1094-2610 (mean ~1980) ppmV in the lower  
388 Da'anzhai Member (early Toarcian age).

389 The evolution and level of  $p\text{CO}_2$  estimated by carbon isotope ratios of the pedogenic carbonates from the GSB compare  
390 favorably with the global composite based on the plant stomata method (data of the composite curve see Table S6), but show  
391 significant differences relative to the global composite  $p\text{CO}_2$  based on paleosols (Fig. 8a. Suchecki et al., 1988; Cerling,  
392 1991; Ekart et al., 1999), which may be attributed to the shortage (<4 samples) of global data and large age uncertainties (Fig.  
393 8a and Table S5 and S6).

394 The changes in  $p\text{CO}_2$  from the GSB, has a similar pattern to coeval seawater temperature estimates through the Early  
395 Jurassic although there are some discrepancies in pace and in detail (comp. Fig. 8a and 8b). That is, the relatively high  $p\text{CO}_2$   
396 1500-2000 ppmV approximately corresponds to the relatively high seawater mean temperature  $-2^\circ\text{C}$  to  $+2^\circ\text{C}$  in the  
397 Sinemurian, low  $p\text{CO}_2$  1000-1500 ppmV corresponds to low seawater mean temperature  $-5^\circ\text{C}$  to  $-2^\circ\text{C}$  in the Pliensbachian,  
398 and quick rising  $p\text{CO}_2$  of 1200 ppmV to ~2500 ppmV corresponds to the rapidly increased seawater temperature of  $-4^\circ\text{C}$  to  
399  $+4^\circ\text{C}$  in the late Pliensbachian-early Toarcian.

400 The  $p\text{CO}_2$  record roughly trends with the carbon isotope records of marine carbonates and organic matter (comp. Fig. 8a to  
401 8d), suggesting a possible linkage of the  $p\text{CO}_2$  record in the GSB to the global carbon cycle (see section 5.2.2). Nevertheless,  
402 it is difficult for the proxies to compare in a higher detail, making it difficult to relate the record to orbital forcing of the  
403 global carbon cycle in the Sinemurian-Pliensbachian (Storm et al., 2020).

404 As a greenhouse gas, atmospheric  $\text{CO}_2$  has a strong control over global temperatures for much of the Phanerozoic (e.g.,  
405 Crowley and Berner, 2001; Royer, 2006; Price et al., 2013), but a decoupling of  $\text{CO}_2$  and temperature has also been  
406 suggested (e.g., Veizer et al., 2000; Dera et al., 2011; Schaller et al., 2011). The pattern of the Early Jurassic  $p\text{CO}_2$   
407 reconstructed from the carbon isotope of pedogenic carbonates in GSB, Southwest China, supports the coupled relationship  
408 of  $\text{CO}_2$ -temperature. Models of the coupling and decoupling of  $\text{CO}_2$ -temperature and  $\text{CO}_2$ -carbon cycle have to consider: 1),  
409 age order of  $\text{CO}_2$ -temperature/carbon cycle relevance, i.e. they should be related in the same age (long term or short term)  
410 hierarchy; 2) precise age constraints of individual  $\text{CO}_2$  and temperature data; 3) methods of  $\text{CO}_2$  and temperature estimates,  
411 depending on precondition, presumptions, parameters, uncertainty, sample diagenesis, etc.; 4) controls or influences of key  
412 factors such ice sheet, tectonic, paleogeography, cosmic ray flux, biota, volcanic eruption, and so on.

### 413 **5.2.2. Rapid $p\text{CO}_2$ falling events**

414 The GSB Early Jurassic  $p\text{CO}_2$  curve reveals two rapid falling events (Fig. 6 and 8a). The first event ( $1E_{\text{CO}_2}$ ) shows a quick  
415 drop from ~2370 ppmV (sample J1z-08-01 at depth 84.7 m) to 1350 ppmV (sample J1z-10-02 at depth 94.4 m) near the  
416 boundary of the Dongyuemiao and Ma'anshan Members (Fig. 6), or to 1075 ppmV (sample J1z-11-02 at depth 111.7 m),  
417 which took place in the early Pliensbachian (~190.4-189.9/189.1 Ma. Fig. 8c). The extent of the rapid falling  $p\text{CO}_2$  is

418 ~1000-1300 ppmV in 9.7-17.0 m. In other words, ~1000 ppmV drop could be accomplished within ~0.5-1.0 Myr based on  
419 the estimate of sedimentation rate (Table S4).

420 While the corresponding early Pliensbachian climatic and isotopic-shifting events are not observed in the smoothed curves of  
421 the Early Jurassic seawater temperature and carbon cycle (Dera et al. 2011), the rapid falling event 1E<sub>CO2</sub> is well correlated  
422 to the nearly coeval excursion events of carbon and oxygen isotopes recorded in western Tethys and North Atlantic (Fig. 8).  
423 The 1E<sub>CO2</sub> compares well to: 1) the rapid carbon isotope negative excursion of (oysters, belemnites, and brachiopods) shells  
424 from the Cleveland Basin, UK (Korte and Hesselbo, 2011) and northwest Algeria (Baghli et al., 2020), 2) that of organic  
425 matter and marine carbonates from southern Pairs Basin (Bougeault et al., 2017; Peti, et al., 2017) and Cardigan Bay Basin,  
426 UK (Storm et al., 2020), and 3) rapid oxygen isotope negative excursion (seawater warming) of belemnites from northern  
427 Spain (van de Schootbrugge et al., 2005). The rapid change of the stable isotope record had been called the  
428 Sinemurian-Pliensbachian boundary event (SPBE) and dated in the ammonite of the upper *Raricostatum* - lower *Jamesoni*  
429 zones (Bougeault et al., 2017).

430 The second event 2E<sub>CO2</sub> displays a large drop of 2574 ppmV (sample J1z-18-01 at depth 252.7 m) to 1094 ppmV (sample  
431 J1z-19-01 at depth 272.3 m), ~1500 ppmV decrease within 19.6 m (estimated age interval ~0.8 Myr. Table S4 and Fig. 8a).  
432 Following the second drop, *p*CO<sub>2</sub> rises rapidly by ~1300 ppmV of 1094 ppmV to 2386 ppmV (sample J1Z-20-01 at depth  
433 294.3 m) although only a few samples support the this cycle of *p*CO<sub>2</sub> falling-rising.

434 Strata in western Sichuan (Xu et al., 2017), may correlate to the time interval of the T-OAE, during which *p*CO<sub>2</sub> doubled  
435 over background values, from ~1000 ppmV to ~2000 ppmV (e.g., Beerling and Royer, 2002; McElwain et al., 2005; Berner,  
436 2006). Given that chronostratigraphical correlation is challenging, the *p*CO<sub>2</sub> falling-rising cycle might correspond to the  
437 quick shifting cycle of stable isotopes during the T-OAE (Fig. 8a and 8c-8d). In detail, the rapid falling-rising of *p*CO<sub>2</sub> is  
438 consistent with: 1) the quick negative-positive carbon isotope excursion of marine carbonates from Italy (Jenkyns and  
439 Clayton, 1986; Sabatino et al., 2009), England and Wales (Jenkyns and Clayton, 1997), north Spain (van de Schootbrugge et  
440 al., 2005), the Lusitanian Basin of Portugal (Hesselbo et al., 2007), Paris Basin (Hermoso et al., 2009), and Morocco (Bodin  
441 et al., 2016); 2) that of invertebrate calcareous shells from the Cleveland Basin of UK (Korte and Hesselbo, 2011) and  
442 northwest Algeria (Baghli et al., 2020); 3) that of marine organic matter from Morocco (Bodin et al., 2016), Yorkshire of  
443 England (Cohen et al., 2004; Kemp et al, 2005), Cardigan Bay Basin of UK (Xu et al., 2018), northern Germany (van de  
444 Schootbrugge et al., 2013), Alberta and British Columbia of Canada (Them II et al., 2017), northern Tibet of China (Fu et al.,  
445 2016), and Japan (Izumi et al., 2018); 4) that of terrestrial organic matter from Sichuan Basin, China (Xu et al., 2017); and 5)  
446 quick oxygen isotope negative-positive shifting (seawater warming) of brachiopods (Suan et al., 2008) and fossil wood  
447 (Hesselbo et al., 2007) from the Lusitanian Basin, Portugal.

448 Multiple hypotheses have been proposed to interpret the 5°-6 °C decrease of sea surface temperatures in the late  
449 Pliensbachian (Bailey et al., 2003; van de Schootbrugge et al., 2005; Suan et al., 2010) and warming ~8 °C in the early



450 Toarcian (Bailey et al., 2003; Suan et al., 2010), such as the sea level falling and rising, methane release, Karoo–Ferrar  
451 eruption, Hispanic corridor opening, etc. Perhaps, these hypotheses somewhat explain the rapid change of sea surface  
452 temperatures, but might not link to drastic falling of  $p\text{CO}_2$ . As we know, atmospheric  $\text{CO}_2$  is controlled by volcanism,  
453 weathering, vegetation on land and phytoplankton in ocean, and orbiting forcing. The Sr isotope curve shows a rapid change  
454 in the early Toarcian but does not in the early Pliensachian (e.g., Jones et al., 1999), indicating a distinct transfer of  
455 weathering took place on the land only at the T-OAE time. No robust evidence shows the rapid changes of terrestrial  
456 vegetation and marine primary productivity for the two intervals except for the floral change in western Tethys during the  
457 T-OAE (Slater et al. 2019). The Karoo–Ferrar eruption could be responsible for the rapid rising of  $p\text{CO}_2$  but not for the  
458 falling. Then the orbital forcing might be an alternative.

459 To sum up, the rapid falling events of the Early Jurassic  $p\text{CO}_2$  values in the GSB, are compatible with the response of stable  
460 isotopes (carbon cycle) and seawater temperature from coeval marine sediments in a total tendency and eventful change, but  
461 not harmonized at a high-resolution time scale. Whatever caused the rapid variations of sea surface temperatures, stable  
462 isotopes, and  $p\text{CO}_2$ , their near concordance suggests that it is a positive feedback of the sea surface temperature and carbon  
463 cycle to the  $p\text{CO}_2$  in trend and event through the Early Jurassic; whereas the higher frequency changes in the  
464 Sinemurian-Pliensbachian might may support other causal driving of the climate, such as orbital forcing (Storm et al., 2020).

## 465 **6. Conclusions**

466 Based on analyses of climate-sensitive sediments and stable isotopes and the reconstruction of paleoclimate and  $p\text{CO}_2$ , we  
467 conclude:

468 1) An overall warm-hot and (semi-) arid climate dominated the GSB during the Early Jurassic, possibly accompanied by  
469 occasional evaporitic climate in the Toarcian. This (semi-) arid climate in GSB is comparable with that in Colorado Plateau,  
470 western America, but distinct from the relatively warm-humid terrestrial climate recognized in other places of Chinese  
471 mainland (e.g., Qaidam, Inner Mongolia, and Lower Yangtze) and the high latitudes of Southern Hemisphere.

472 2) The Early Jurassic  $p\text{CO}_2$  values show that a range between 980 ppmV and 2610 ppmV is  $\sim 3.5$ -10 times the pre-industrial  
473 value 275 ppmV and the mean 1720 ppmV is  $\sim 6$  times the pre-industrial value. Three phases of  $p\text{CO}_2$  values were  
474 distinguished: 1500-2000 (mean  $\sim 1700$ ) ppmV in the Sinemurian age, 1000-1500 (mean  $\sim 1300$ ) ppmV in the Pliensbachian  
475 age, and 1094-2610 (mean  $\sim 1980$ ) ppmV in the early Toarcian. Two events of rapidly falling  $p\text{CO}_2$  were also recognized:  
476  $\sim 1000$ -1300 ppmV drop at the Sinemurian-Pliensbachian boundary and quick falling (-rising) by  $\sim 1500$  ppmV in the early  
477 Toarcian. The phases and events manifest the perturbation of  $p\text{CO}_2$  in the Early Jurassic.

478 3) The perturbation and rapid falling events of the Early Jurassic  $p\text{CO}_2$  from the GSB are compatible with the carbon cycle  
479 and seawater temperature from coeval marine sediments in the North Atlantic and western Tethys in a total tendency and

480 eventful change. The compatibility suggests that it is a positive linkage of the sea surface temperature and carbon cycle to  
481 the  $p\text{CO}_2$  through the Early Jurassic. On the contrary, differences at a high-resolution time scale implies additional climate  
482 drivers, such as orbital forcing are important in the Sinemurian-Pliensbachian record.

### 483 **Acknowledgements**

484 We thank Professors Helmut Weissert and Dan Breecker for careful scrutiny, constructive comments and suggestions. It is  
485 acknowledged this research was supported by Natural Science Foundation of China (NSFC) project 41672097.

486

### 487 **References**

- 488 Alonso-Zarza, A M. and Tanner, L. H.: Preface. *Geol. Soc. Am. Spe. Pap.*, 416, v-vii, doi, 10.1130/0-8137-2416-3.v, 2006.
- 489 Arabas, A., Schlogl, J., and Meiste C.: Early Jurassic carbon and oxygen isotope records and seawater temperature variations:  
490 Insights from marine carbonate and belemnite rostra (Pieniny Klippen Belt, Carpathians), *Palaeogeogr. Palaeoclimatol.*  
491 *Palaeoecol.*, 485, 119–135, 2017
- 492 Arens, N. C., Jahren, A. H., and Amundson, R.: Can  $\text{C}_3$  plants faithfully record the carbon isotopic composition of  
493 atmospheric carbon dioxide, *Paleobiology*, 26, 137–164, 2000,
- 494 Arias, C.: Extinction pattern of marine Ostracoda across the Pliensbachian-Toarcian boundary in the Cordillera Ibérica, NE  
495 Spain: Causes and consequences, *Geobios*, 42, 1-15, 2009.
- 496 Baghli, H., Mattioli, E., Spangenberg, J. E., Bensalah, M., Arnaud-Godet, F., Pittet, B., and Suan, G.: Early Jurassic climatic  
497 trends in the south-Tethyan margin. *Gondwana. Res.*, 77, 67-81, doi, 10.1016/j.gr.2019.06.016, 2020.
- 498 Bailey, T. R., Rosenthal, Y., McArthur, J. M., van de Schootbrugge, B., and Thirlwall, M. F.: Paleoceanographic changes of  
499 the Late Pliensbachian-Early Toarcian interval: a possible link to the genesis of an Oceanic Anoxic Event, *Earth Planet.*  
500 *Sci. Lett.*, 212, 307-320, 2003.
- 501 Beerling, D. J. and Royer, D. L.: Reading a  $\text{CO}_2$  signal from fossil stomata, *The New Phytologist*, 153, 387-397, doi:0.  
502 1046/j. 0028-646X. 2001. 00335. x, 2002.
- 503 Berner, R. A.: GEOCARBSULF: A combined model for Phanerozoic atmospheric  $\text{O}_2$  and  $\text{CO}_2$ , *Geochi. Cosmochi. Ac.*,  
504 70(23 Spec. Iss. ), 5653-5664, 2006.
- 505 Besse, J., and Courtillot, V.: Paleogeographic maps of the continents bordering the Indian Ocean since the Early Jurassic: J.  
506 *Geophys. Res.*, 93, 11791–808, 1988.
- 507 Blakey, R. C., Peterson, F., and Kocurek, G.: Synthesis of late Paleozoic and Mesozoic eolian deposits of the Western  
508 Interior of the United States, *Sediment. Geol.*, 56, 3-125, doi, [https://doi.org/10.1016/0037-0738\(88\)90050-4](https://doi.org/10.1016/0037-0738(88)90050-4), 1988.

- 509 Bodin, S., Krencker, F. N., Kothe, T., Hoffmann, R., Mattioli, E., Heimhofer, U., and Kabiri, L.: Perturbation of the carbon  
510 cycle during the late Pliensbachian – early Toarcian: New insight from high-resolution carbon isotope records in  
511 Morocco, *J. Afr. Earth Sci.*, 116, 89–104, doi, 10.1016/j.jafrearsci.2015.12.018, 2016.
- 512 Boucot, A. J., Chen, X., Scotese, C. R., and Morley, R. J.: Phanerozoic Paleoclimate: An Atlas of Lithologic Indicators of  
513 Climate, *SEPM Concepts in Sedimentology and Paleontology* 11. SEPM, Tulsa, 1-478, 2013.
- 514 Bougeault, C., Pellenard, P., Deconinck, J. F., Hesselbo, S. P., Dommergues, J. L., Bruenau, L., Cocquerez, T., Laffont, R.,  
515 Huret, E., and Thibault, N.: Climatic and palaeoceanographic changes during the Pliensbachian (Early Jurassic) inferred  
516 from clay mineralogy and stable isotope (C-O) geochemistry (NW Europe), *Global Planet. Change*, 149, 139-152,  
517 2017.
- 518 Breecker, D. O. and Retallack, G. J.: Refining the pedogenic carbonate atmospheric CO<sub>2</sub> proxy and application to Miocene  
519 CO<sub>2</sub>, *Palaeogeogr. Palaeoclimatol. Palaeoecol.*, 406, 1-8, 2014.
- 520 Breecker, D. O., Sharp, Z. D., and McFadden, L. D.: Atmospheric CO<sub>2</sub> concentrations during ancient greenhouse climates  
521 were similar to those predicted for A. D. 2100, *PNAS*, 107, 2, 576-580, 2009.
- 522 Breecker, D. O., Sharp, Z. D., and McFadden, L. D.: Seasonal bias in the formation and stable isotope composition of  
523 pedogenic carbonate in modern soil from central New Mexico, USA, *Geol. Soc. Am. Bull.*, 12, 630-640, 2010.
- 524 Breecker, D. O.: Quantifying and understanding the uncertainty of atmospheric CO<sub>2</sub> concentrations determined from calcic  
525 paleosols. *Geochem. Geophys. Geosyst.*, 14, 3210–3220, 2013.
- 526 Bromley, M.: Topographic inversion of early interdune deposits, Navajo Sandstone (Lower Jurassic), Colorado Plateau,  
527 USA, *Sediment. Geol.*, 80, 1-25, 1992.
- 528 Buchmann, N., Brooks, R. J., Flanagan, L. B., and Ehleringer, J. R.: Carbon isotope discrimination of terrestrial ecosystems.  
529 In Griffiths, H., ed. *Stable Isotopes: Integration of Biological, Ecological and Geochemical Processes*, BIOS Scientific  
530 Publications, Oxford, United Kingdom, 203–21, 1998.
- 531 Caruthers, A. H., Smith, P. L., Gröcke, D. R.: The Pliensbachian-Toarcian (Early Jurassic) extinction, a global multi-phased  
532 event, *Palaeogeogr. Palaeoclimatol. Palaeoecol.*, 386, 104-118, 2013.
- 533 Cerling, T. E.: Carbon dioxide in the atmosphere: evidence from Cenozoic and Mesozoic paleosols: *Am. J. Sci.*, 291,  
534 377-400, 1991.
- 535 Cerling, T. E.: Stable carbon isotopes in palaeosol carbonates, in: *Palaeoweathering, palaeosurfaces and related continental*  
536 *deposits*, edited by: Thiry, M. and Simm-Coinçon, R., *Spec. P. Intl. Asso. Sedi.*, 27, 43-60, 1999.
- 537 Cleveland, D. M., Nordt, L. C., Dworkin, S. I., and Atchley, S. C.: Pedogenic carbonate isotopes as evidence for extreme  
538 climatic events preceding the Triassic-Jurassic boundary: implications for the biotic crisis? *GSA Bull.*, 120, 1408-1415,  
539 2008.
- 540 Cohen, K. M., Finney, S. C., Gibbard, P. L., and Fan, J. X. *The ICS International Chronostratigraphic Chart (2013 updated)*.

541 Episodes, 36, 199-204, 2013.

542 Cohen, A. S., Coe, A. L., Harding, S. M., and Schwark, L.: Osmium isotope evidence for the regulation of atmospheric CO<sub>2</sub>  
543 by continental weathering, *Geology*, 32, 157–160, 2004.

544 Crowley, T. J. and Berner, R. A.: CO<sub>2</sub> and climate change, *Science*, 292, 870–872, 2001.

545 Deng, S. H., Zhao, Y., Lu, Y. Z., Shang, P., Fan, R., Li, X., Dong, S. X., and Liu, L.: Plant fossils from the Lower Jurassic  
546 coal-bearing formation of central InnerMongolia of China and their implications for palaeoclimate, *Palaeoworld*, 26:  
547 279-316, 2017.

548 Dera, G., Brigaud, B., Monna, F., Laffont, R., Pucéat, E., Deconinck, J. F., Pellenard P., Joachimski, M. M., and Durlet, C.:  
549 Climatic ups and downs in a disturbed Jurassic world, *Geology*, 39(3), 215-218, 2011.

550 Dera, G., Pellenard, P., Neige, P., Deconinck, J. F., Pucéat, E., and Dommergues, J. L.: Distribution of clay minerals in Early  
551 Jurassic Peritethyan seas: Palaeoclimatic significance inferred from multiproxy comparisons, *Palaeogeogr.*  
552 *Palaeoclimatol. Palaeoecol.*, 271(1-2), 39–51, doi, 10.1016/j.palaeo.2008.09.010, 2009.

553 Dong, Z. M.: A new prosauropod from Ziliujing Formation of Sichuan Basin, *Verte. Palasiatica*, 22(4), 310-313, 1984 (in  
554 Chinese with English abstract).

555 Duan, S. Y. and Chen, Y.: Mesozoic fossil plants and coal formation of eastern Sichuan Basin, in: *Continental Mesozoic*  
556 *Stratigraphy and Paleontology in Sichuan Basin of China: Part II, Paleontological Professional Papers*, People's Publ.  
557 House Sichuan, Chengdu, 491-519, 1982 (in Chinese).

558 Ekart, D. D., Cerling, T. E., Montñez, I. P., and Tabor, N. J.: A 400 million year carbon isotope record of pedogenic  
559 carbonate: implications for paleoatmospheric carbon dioxide, *Am. J. Sci.*, 299, 805-827, 1999.

560 Flügel, E.: *Microfacies of Carbonate Rocks: Analysis, Interpretation and Application*, Springer-Verlag, Berlin, Heidelberg,  
561 New York, 976 pp. 2004.

562 Friedli, H., Lotscher, H., Oeschger, H., Siegenthal, U., and Stauffer, B.: Ice core record of the <sup>13</sup>C/<sup>12</sup>C ratio of atmospheric  
563 CO<sub>2</sub> in the past two centuries, *Nature*, 324, 237–238, 1986.

564 Fu, X. G., Wang, J., Feng, X. L., Wang, D., Chen, W. B., Song, C. Y., and Zeng, S. Q.: Early Jurassic carbon-isotope  
565 excursion in the Qiangtang Basin (Tibet), the eastern Tethys: implications for the Toarcian Oceanic anoxic event, *Chem.*  
566 *Geol.*, 442, 67–72, 2016.

567 Gómez, J. J., and Goy, A.: Warming-driven mass extinction in the Early Toarcian (Early Jurassic) of northern Spain,  
568 Correlation with other time-equivalent European sections. *Palaeogeogr. Palaeoclimatol. Palaeoecol.*, 306, 176-195,  
569 2011.

570 Gómez, J. J., Comas-Rengifo, M. J., and Goy, A.: Palaeoclimatic oscillations in the Pliensbachian (Early Jurassic) of the  
571 Asturian Basin (Northern Spain), *Clim. Past*, 12, 1199-1214, 2015.

572 Gómez, J. J., Goy, A., and Canales, M. L.: Seawater temperature and carbon isotope variations 15 in belemnites linked to

573 mass extinction during the Toarcian (Early Jurassic) in Central and Northern Spain. Comparison with other European  
574 sections, *Palaeogeogr. Palaeoclimatol. Palaeoecol.*, 258, 28-58, 2008.

575 Guo, L. Y., Zhang, S. W., Xie, X. N., Li, Z. S., Huang, C. Y., and Chen, B. C.: Geochemical characteristics and organic  
576 matter enrichment of the Dongyuemiao Member mudstone of Lower Jurassic in the Western Hubei-Eastern Chongqing,  
577 *Ear. Sci.*, 42(7): 1235-1246, 2017 (in Chinese with English abstract).

578 Guo, Z. W, Deng, K. L., and Han, Y. H.: Formation and Evolution of the Sichuan Basin, Geo. Publ. House, Beijing, 200,  
579 1996.

580 Hallam, A., and Wignall, P. B.: Mass extinctions and sea-level changes, *Earth Sci. Rev.*, 48, 217-250, 1999.

581 He, T. H. and Liao, C. F.: Control of Upper Triassic division and correlation and Indosinian Movement on oil and gas  
582 accumulation in Sichuan Basin, *Acta Geol. Sichuan*, 00, 40-55, 1985 (in Chinese).

583 Hermoso, M., Le Callonnec, L., Minoletti, F., Renard, M., and Hesselbo, S. P.: Expression of the Early Toarcian negative  
584 carbon-isotope excursion in separated carbonate microfractions (Jurassic, Paris Basin), *Earth Planet. Sci. Lett.*, 277,  
585 194-203, 2009.

586 Hesselbo, S. P. and Jenkyns, H. C.: British Lower Jurassic sequence stratigraphy, in: *Mesozoic-Cenozoic Sequence*  
587 *Stratigraphy of European Basins*, edited by: de Graciansky, P. C., Hardenbol, J., Jacquin, Th., and Vail, P. R., *SEPM*  
588 *Spec. Pap.*, 60, 562-581, 1998.

589 Hesselbo, S. P., Gröcke, D. R., Jenkyns, H. C., Bjerrum, C. J., Farrimond, P., Morgans Bell, H. S., Green, O. R.: Massive  
590 dissociation of gas hydrate during a Jurassic oceanic anoxic event, *Nature*, 406, 392-395, doi:10.1038/35019044.,  
591 2000.

592 Hesselbo, S. P., Jenkyns, H. C., Duarte, L. V., and Oliveira, L. C. V.: Carbon-isotope record of the Early Jurassic (Toarcian)  
593 Oceanic Anoxic Event from fossil wood and marine carbonate Lusitanian Basin, Portugal, *Earth Planet. Sci. Lett.*, 253,  
594 455-470, 2007.

595 Huang, P., Guan, Y. M., and Yang, X. Q.: Early Jurassic palynoflora from a drilling section of Jurong, Jiangsu, *Acta*  
596 *Micropalaeontol. Sin.*, 17(1), 85- 98, 2000.

597 Huang, C. J., and Hesselbo, S. P.: Pacing of the Toarcian Oceanic Anoxic Event (Early Jurassic) from astronomical  
598 correlation of marine sections. *Gondwana Res.*, 25, 1348-1356, doi, org/10.1016/j.gr.2013.06.023, 2014.

599 Huang, Q. S.: Paleoclimate and coal-forming characteristics of the Late Triassic Xujiahe stage in northern Sichuan, *Geol.*  
600 *Rev.*, 41(1): 92-99, 1995, (in Chinese with English abstract).

601 Huang, Q. S.: The flora and paleoenvironment of the Early Jurassic Zhenzhuchong Formation in Daxian-Kaixian region,  
602 northern margin of the Sichuan Basin, *Ear. Sci. J. China Uni. Geosci.*, 3, 221-229, 2001 (in Chinese with English  
603 abstract).

604 Imbellone, P. A.: Classification of Paleosols. São Paulo, UNESP, *Geociências*, 30(1), 5-13, 2011,

605 Izumi, K., Kemp, D., Itamiya, S., and Inui, M.: Sedimentary evidence for enhanced hydrological cycling in response to rapid  
606 carbon release during the early Toarcian oceanic anoxic event, *Earth Planet. Sci. Lett.*, 481, 162–170, 2018.

607 Jahren, A. H., Arens, N. C., and Harbeson, S. A.: Prediction of atmospheric  $\delta^{13}\text{C}_{\text{CO}_2}$  using fossil plant tissues, *Rev. Geophys.*,  
608 46, RG1002, doi: 10.1029/2006RG000219, 2008.

609 Jenkyns, H. C. and Clayton, C. J.: Black shales and carbon isotopes in pelagic sediments from the Tethyan Lower Jurassic,  
610 *Sedimentology*, 33, 87-106, 1986.

611 Jenkyns, H. C., and Clayton, C. J., Lower Jurassic epicontinental carbonates and mudstones from England and Wales:  
612 chemostratigraphic signals and the early Toarcian anoxic event, *Sedimentology*, 44, 687-706, 1997.

613 Jenkyns, H. C., Jones, C. E., Gröcke, D. R., Hesselbo, S. P., and Parkinson, D. N.: Chemostratigraphy of the Jurassic System:  
614 Applications, limitations and implications for palaeoceanography, *J. Geol. Soc. London*, 159, 351-378, 2002.

615 Jenkyns, H. C.: Geochemistry of oceanic anoxic events, *Geochem. Geophys. Geosyst.*, 11, Q03004. doi:10.  
616 1029/2009GC002788, 2010.

617 Jones, C. E., Jenkyns, H. C., and Hesselbo, S. P.: Strontium isotopes in Early Jurassic seawater: *Geoch. Cosmoch. Acta*, 58,  
618 1285–1301, 1994.

619 Kemp, D. B., Coe, A. L., Cohen, A. S., and Schwark, L.: Astronomical pacing of methane release in the Early Jurassic  
620 period, *Nature*, 437, 396-399, doi, org/10.1038/nature04037, 2005.

621 Kenny, R.: A cool time in the Early Jurassic: first continental palaeoclimate estimates from oxygen and hydrogen isotope  
622 ratios in chert from Navajo Sandstone carbonate lenses, Utah (USA), *Carbonate Evaporite*, doi,  
623 10.1007/s13146-015-0276-z, 2015.

624 Kent, D. V., Olsen, P. E., and Muttoni, G.: Astrochronostratigraphic polarity time scale (APTS) for the Late Triassic and  
625 Early Jurassic from continental sediments and correlation with standard marine stages, *Earth-Sci. Rev.*, 166, 153-180,  
626 2017.

627 Korte, C., and Hesselbo, S. P.: Shallow marine carbon and oxygen isotope and elemental records indicate  
628 icehouse-greenhouse cycles during the Early Jurassic, *Paleoceanography*, 26, 1–18, 2011.

629 Korte, C., Hesselbo, S. P., Jenkyns, H. C., Rickaby, R. E. M., and Spötl, C.: Palaeoenvironmental significance of carbon-  
630 and oxygen-isotope stratigraphy of marine Triassic-Jurassic boundary sections in SW Britain, *J. Geol. Soc. London*,  
631 166(3), 431-445, 2009.

632 Korte, K., Hesselbo, S. P., Ullmann, C.V., Dietl, G., Ruhl, M., Schweigert, G., Thibault, N.: Jurassic climate mode governed  
633 by ocean gateway, *Nat. Commun.*, 6, 10015, doi, 10.1038/ncomms10015, 2015.

634 Li, H. C. and Ku, T. L.:  $\delta^{13}\text{C}$ - $\delta^{18}\text{O}$  covariance as a paleohydrological indicator for closed basin lakes, *Palaeogeogr.*  
635 *Palaeoclimatol. Palaeoecol.*, 133, 69-80, 1997.

636 Li, L. Q., Wang, Y. D., Liu, Z. S., Zhou, N., and Wang, Y.: Late Triassic palaeoclimate and palaeoecosystem variations

637 inferred by palynological record in the northeastern Sichuan Basin, China, *Paläontol. Zeits.*, 309-324, DOI 10.  
638 1007/s12542-016-0309-5, 2016.

639 Li, W. M. and Chen, J. S.: Discovery and significances of the Jurassic Ziliujing Formation in Tianzhu, Guizhou, China *New*  
640 *Techn. Prod.*, 13, 134-135, 2010 (in Chinese).

641 Li, X. B. and Meng, F. S.: Discovery of fossil plants from the Ziliujing Formation in Hechuan of Chongqing. *Geol. Min.*  
642 *Resour. South China*, 3: 60-65, 2003 (in Chinese with English abstract).

643 Li, Y. Q. and He, D. F.: Evolution of tectonic-depositional environment and prototype basins of the Early Jurassic in Sichuan  
644 Basin and adjacent areas, *Acta Petrol. Sin.*, 35(2), 219-232, 2014 (in Chinese with English abstract).

645 Li, Y., Allen, P. A., Densmore, A. L., and Xu, Q.: Evolution of the Longmen Shan Foreland Basin (Western Sichuan, China)  
646 during the Late Triassic Indosinian Orogeny. *Basin Res.*, 15, 117-138, 2003.

647 Liang, B., Wang, Q. W., and Kan, Z. Z.: Geochemistry of Early Jurassic mudrocks from Ziliujing Formation and  
648 implications for source-area and weathering in dinosaur fossils site in Gongxian, Sichuan province, *J. Min. Petr.*, 26(3),  
649 94-99, 2006 (in Chinese with English abstract).

650 Littler, K., Hesselbo, S. P., and Jenkyns, H. C.: A carbon-isotope perturbation at the Pliensbachian-Toarcian boundary:  
651 evidence from the Lias Group, NE England. *Geol. Mag.*, 147, 181-192, 2010.

652 Liu, J. L., Ji, Y. L., Zhang, K. Y., Li, L. D., Wang, T. Y., Yang, Y., and Zhang, J.: Jurassic sedimentary system transition  
653 and evolution model in western Sichuan Foreland Basin, *Acta Petrol. Sin.*, 37(6), 743-756, 2016 (in Chinese with  
654 English abstract).

655 Ma, Y. S., Chen, H. D., Wang, G. L., Guo, T. L., Tian, J. C., Liu, W. J., Xu, X. S., Zheng, R. C., Mou, C. L., and Hou, M. C.:  
656 *Atlas of Lithofacies Paleogeography on the Sinian-Neogene Tectonic-Sequence in South China*, Science Press, Beijing,  
657 162-165, 2009 (in Chinese).

658 Mack, G. H. and James, W. C.: Paleoclimate and the Global Distribution of Paleosols, *J. Geol.*, 102, 360-366, 1994.

659 Mack, G. H., James, W. C., and Monger, H. C.: 1 Classification of paleosols, *Geol. Soc. Am. Bull.*, 105, 129-136, 1993.

660 McElwain, J. C., Wade-Murphy, J., and Hesselbo, S. P.: Changes in carbon dioxide during an oceanic anoxic event linked to  
661 intrusion into Gondwana coals, *Nature*, 435, 479-482, doi:org/10. 1038/nature03618, 2005.

662 McKenzie, J. A., and Vasconcelos C.: Dolomite Mountains and the origin of the dolomite rock of which they mainly consist:  
663 historical developments and new perspectives, *Sedimentology*, 56, 205 - 219, doi, 10.1111/j.1365-3091.2008.01027.x,  
664 2009.

665 Meng, F. S., Chen, H. M., and Li, X. B.: Study on Lower Middle Jurassic boundary in Chongqing region, *Geol. Min. Resour.*  
666 *S China*, 3, 64-71, 2005 (in Chinese with English abstract).

667 Meng, F. S., Li, X. B., and Chen, H. M.: Fossil plants from Dongyuemiao Member of the Ziliujing Formation and  
668 Lower-Middle Jurassic boundary in Sichuan basin, China, *Acta Palaeontol. Sin.*, 42(4), 525-536, 2003. (in Chinese with

669 English abstract).

670 Metodiev, L. and Koleva-Rekalova, E.: Stable isotope records ( $\delta^{18}\text{O}$  and  $\delta^{13}\text{C}$ ) of Lower - Middle Jurassic belemnites from  
671 the Western Balkan mountains (Bulgaria), Palaeoenvironmental application, *Appl. Geochem.*, 23, 2845–2856, 2008.

672 Mintz, J. S., Driese, S. G., Breecker, D. O., and Ludvigson, G. A.: Influence of changing hydrology on pedogenic calcite  
673 precipitation in Vertisols, Dance Bayou, Brazoria County, Texas, USA: implications for estimating paleoatmospheric  
674  $p\text{CO}_2$ , *J. Sedi. Res.*, 81(6), 394-400, 2011.

675 Mo, Y. Z. and Yu, H. Y.: The discovery and its geological significance of dolomite in Ziliujing Groups of Middle and Lower  
676 Jurassic Series in Ma'anshan Member, *Geol Guizhou*, 10(1), 110-113, 1987 (in Chinese with English abstract).

677 Montañez, I. P.: Modern soil system constraints on reconstructing deep-time atmospheric  $\text{CO}_2$ , *Geochim. Cosmochim. Acta*,  
678 101, 57–75, 2013.

679 Nadelhofer K. J., and Fry B.: Controls on natural nitrogen-15 and carbon-13 abundances in forest soil organic matter, *Soil*  
680 *Sci. Soc. Am. J.*, 52, 1633-1640, 1988.

681 Newport, R., Hollis, C., Bodin, S., and Redfern, J.: Examining the interplay of climate and low amplitude sea-level change  
682 on the distribution and volume of massive dolomitization: Zebbag Formation, Cretaceous, Southern Tunisia, *Deposit.*  
683 *Rec.*, 3(1), 38–59, doi,10.1002/dep2.25, 2017.

684 Parrish, J. T., Hasiotis, S. T., and Chan, M. A.: Carbonate deposits in the Lower Jurassic Navajo Sandstone, southern Utah  
685 and northern Arizona, *J. Sedi. Res.*, 87, 740-762, doi, <https://doi.org/10.2110/jsr.2017.42>, 2017.

686 Parrish, J. T., Rasbury, E. T., Chan, M. A., and Hasiotis, S. T.: Earliest Jurassic U-Pb ages from carbonate deposits in the  
687 Navajo Sandstone, southeastern Utah, USA, *Geology*, 47(11), 1015–1019, doi, 10.1130/g46338.1, 2019.

688 Peng, G. Z.: Assemblage characters of Jurassic dinosaurian fauna in Zigong of Sichuan, *J. Geosci.*, 33(2), 113-123, 2009 (in  
689 Chinese with English abstract).

690 Peti, L., Thibault, N., Clémence, M. E., Korte, C., Dommergues, J. L., Bougeault, C., Pellenard, P., Jelby, M. E., and  
691 Ullmann, C. V.: Sinemurian-Pliensbachian Calcareous Nannofossil Biostratigraphy and Organic Carbon Isotope  
692 Stratigraphy in the Paris Basin: Calibration to the Ammonite Biozonation of NW Europe, *Palaeogeogr. Palaeoclimatol.*  
693 *Palaeoecol.*, 468, 142–161, 2017.

694 Petrash, D. A., Bialik, O. M., Bontognali, T. R. R., Vasconcelos, C., Roberts, J. A., McKenzie, J. A., and Konhauser, K. O.:  
695 Microbially catalyzed dolomite formation: From near-surface to burial, *Earth Sci. Rev.*, 171, 558–582, doi,  
696 10.1016/j.earscirev.2017.06.015, 2017.

697 Philippe M., Puijalon S., Suan G., Mousset S., Thévenard F., and Mattioli E.: The palaeolatitudinal distribution of fossil  
698 wood genera as a proxy for European Jurassic terrestrial climate, *Palaeogeogr. Palaeoclimatol. Palaeoecol.*, 466, 373–  
699 381, 2017.

700 Pole, M.: Vegetation and climate of the New Zealand Jurassic, *GFF*, 131:1-2, 105-111, DOI: 10. 1080/11035890902808948,



701 2009.

702 Price, G. D., Twitchett, R. J., Wheeley, J. R., and Buono, G.: Isotopic evidence for long term warmth in the Mesozoic, *Sci.*  
703 *Rep.*, 3, 1438, doi, 10.1038/srep01438, 2013.

704 Qian, T., Liu, S. F., Wang, Z. X., Li, W. P., and Chen, X. L.: Characteristics of the Baitianba Formation conglomerate of  
705 Lower Jurassic in the northern Sichuan basin and its constraint to the uplift of the south Dabashan, *China Sci. Paper*,  
706 11(21), 2402-2408, 2016 (in Chinese with English abstract).

707 Rees, P. A., Zeigler, A. M., and Valdes, P. J.: Jurassic phytogeography and climates: new data and model comparisons, in:  
708 *Warm Climates in Earth History*, edited by: Huber, B., MacLeod, K., and Wing, S., Cambridge University Press, 297–  
709 318, 1999.

710 Retallack, G. J.: A 300-million-year record of atmospheric carbon dioxide from fossil plant cuticles, *Nature*, 411, 287-290,  
711 2001a.

712 Retallack, G. J.: Adapting soil taxonomy for use with paleosols. *Quatern. Int.*, 51/52: 55-57, doi,  
713 10.1016/S1040-6182(98)00039-1, 1998.

714 Retallack, G. J.: *Soils of the Past--An Introduction to Paleopedology*, Blackwell Science Ltd, Oxford, 333, 2001b.

715 Riding, J. B., Leng, M. J., Kender, S., Hesselbo, S. P., and Feist-Burkhardt, S.: Isotopic and palynological evidence for a new  
716 Early Jurassic environmental perturbation, *Palaeogeogr. Palaeoclimatol. Palaeoecol.*, 374: 16–27, 2013.

717 Robinson, S. A., Andrews, J. E., Hesselbo, S. P., Radley, J. D., Dennis, P. F., Harding, I. C., and Allen, P.: Atmospheric  
718  $p\text{CO}_2$  and depositional environment from stable-isotope geochemistry of calcrite nodules (Barremian, Lower  
719 Cretaceous, Wealden Beds, England), *J. Geol. Soc., London*, 159, 215–24, 2002.

720 Robinson, S. A., Ruhl, M., Astley, D. L., Naafs, B. D. A., Farnsworth, A. J., Bown, P. R., Jenkyns, H. C., Lunt D. J.,  
721 O'Brien, C., Pancost, R. D., and Markwick, P. J.: Early Jurassic North Atlantic sea-surface temperatures from TEX86  
722 palaeothermometry. *Sedimentology*, 64(1), 215–230, doi, 10.1111/sed.12321, 2017.

723 Romanek, C., Grossman, E. and Morse, J.: Carbon isotopic fractionation in synthetic aragonite and calcite: effects of  
724 temperature and precipitation rate, *Geochim. Cosmochim. Ac.*, 56, 419-430, 1992.

725 Rosales, I., Quesada, S., and Robles, S.: Primary and diagenetic isotopic signals in fossils and hemipelagic carbonates: the  
726 Lower Jurassic of northern Spain, *Sedimentology*, 48, 1149–1169, 2001.

727 Royer, D. L.: CO<sub>2</sub>-forced climate thresholds during the Phanerozoic: *Geochim. Cosmochim. Ac.*, 70, 56, 65–75, doi: 10.  
728 1016/j.gca.2005.11.031, 2006.

729 Sabatino, N., Neri, R., Bellanca, A., Jenkyns, H., Baudin, F., Parisi, G., and Masetti, D.: Carbon isotope records of the Early  
730 Jurassic (Toarcian) oceanic anoxic event from the Valdorbia (Umbria-Marche Apennines) and Monte Mangart (Julian  
731 Alps) sections: palaeogeographic and stratigraphic implications, *Sedimentology*, 56, 1307-1328, 2009.

732 SBG (Sichuan Bureau of Geology): *Reports of 1:200,000 Regional Geology Investigations (Profile Qianjiang)*, 48, 1975 (in

733 Chinese).

734 SBG (Sichuan Bureau of Geology): Reports of 1:200,000 Regional Geology Investigations (Profile Xuyong), 55, 1976 (in  
735 Chinese).

736 SBG (Sichuan Bureau of Geology): Reports of 1:200,000 Regional Geology Investigations (Profiles Suining, Zigong,  
737 Neijiang, Yibin, and Luzhou), 43-50, 1980a (in Chinese).

738 SBG (Sichuan Bureau of Geology): Reports of 1:200,000 Regional Geology Investigations (Profiles Yilong, Tongjiang,  
739 Nanchong, Guang'an, and Chongqing), 100-101, 1980b (in Chinese).

740 SBGM (Sichuan Bureau of Geology and Mineral Resources): Geology of Sichuan Province, Geol. Publ. House, Beijing, 730,  
741 1991 (in Chinese with English summary).

742 SBGM: Lithostratigraphy of Sichuan Province, China Uni. Geosci. Press, Wuhan, 388, 1997 (in Chinese).

743 Schaller, M. F., Wright, J. D., and Kent, D. V.: Atmospheric  $p\text{CO}_2$  perturbations associated with the Central Atlantic  
744 Magmatic Province, *Science*, 331, 1404-1409, doi, 10.1126/science.1199011, 2011.

745 Sellwood, B. W., and Valdes, P. J.: Jurassic climates, *P. Geologist Assoc.*, 119, 5-17, 2008.

746 Scotese, C. R.: Atlas of Jurassic Paleogeographic Maps, PALEOMAP Atlas for ArcGIS, volume 4, The Jurassic and Triassic,  
747 Maps 32-42, Mollweide Projection, PALEOMAP Project, Evanston, IL, 2014.

748 Slater, S. M., Twitchett, R. J., Danise, S., and Vajda, V.: Substantial vegetation response to Early Jurassic global warming  
749 with impacts on oceanic anoxia, *Nature Geo.*, doi, 10.1038/s41561-019-0349-z, 2019.

750 Soil survey Staff: Keys to Soil Taxonomy, Pocahontas Press, Blacksburg, VA, 1998.

751 Steinhorsdottir, M. and Vajda, V.: Early Jurassic (late Pliensbachian)  $\text{CO}_2$  concentrations based 5 on stomatal analysis of  
752 fossil conifer leaves from eastern Australia, *Gondwana Res.* 27, 829-897, 2015.

753 Storm, M. S., Hesselbo, S. P., Jenkyns, H. C., Ruhl, M., Ullmann, C. V., Xu, W., Leng, M. J., Riding, J. B., Gorbanenko, O.:  
754 Orbital pacing and secular evolution of the Early Jurassic carbon cycle. *PNAS*, 117(8), 3974-3982, doi,  
755 10.1073/pnas.1912094117, 2020.

756 Suan, G., Mattioli, E., Pittet, B., Lécuyer, C., Suchéras-Marx, B., Duarte, L. V., Philippe, M., Reggiani, L., and Martineau, F.:  
757 Secular environmental precursors to Early Toarcian (Jurassic) extreme climate changes, *Earth Planet. Sci. Letts.*, 290,  
758 448-458, doi, org/10. 016/j.epsl.2009.12.047, 2010.

759 Suan, G., Mattioli, E., Pittet, B., Mailliot, S., and Lécuyer, C.: Evidence for major environmental perturbation prior to and  
760 during the Toarcian (Early Jurassic) oceanic anoxic event from the Lusitanian Basin, Portugal, *Paleoceanography*, 23,  
761 PA1202, doi, org/10. 1029/2007PA001459, 2008.

762 Talbot, M. R.: A review of the palaeohydrological interpretation of carbon and oxygen isotopic ratios in primary lacustrine  
763 carbonates. *Chem. Geol. (Isotope Geoscience Section)*, 80, 261-2791, 1990.

764 Tanner, L. H., and Lucas, S. The Whitmore Point Member of the Moenave Formation: Early Jurassic Dryland Lakes on the

- 765 Colorado Plateau, Southwestern USA, *Volum. Jur.*, 6(6), 11-21, 2008.
- 766 Tanner, L. H., Hubert, J. F., Coffey, B. P., and McInerney, D. P.: Stability of atmospheric CO<sub>2</sub> levels across the  
767 Triassic/Jurassic boundary, *Nature*, 411, 675-677, 2001.
- 768 Them, TR, II, Gill, B. C., Caruthers, A. H., Gröcke, D. R., Tulsy, E. T., Martindale, R. C., Poulton, T. P., and Smit, P. L.:  
769 High-resolution carbon isotope records of the Toarcian oceanic anoxic event (Early Jurassic) from North America and  
770 implications for the global drivers of the Toarcian carbon cycle, *Earth Planet. Sci. Lett.*, 459, 118–126, 2017.
- 771 Tramoy, R., Schnyder, J., Nguyen, Tu T. T., Yans, J., Jacob, J., Sebilo, M., Derenne, S., Philippe, M., Huguet, A., Pons, D.,  
772 and Baudin, F.: The Pliensbachian-Toarcian paleoclimate transition: New insights from organic geochemistry and C, H,  
773 N isotopes in a continental section from Central Asia, *Palaeogeogr. Palaeoclimatol. Palaeoecol.*, 461, 310–327, 2016.
- 774 Tucker, M. E.: *Sedimentary rocks in the field - a practical guide* (4th ed.), Wiley-Blackwell, Chichester, England, 276 pp,  
775 2011.
- 776 Vandeginste, V., and John, C. M.: Influence of climate and dolomite composition on dedolomitization: insights from a  
777 multi-proxy study in the central Oman Mountains, *J. Sediment. Res.*, 82(3), 177-195, doi, 10.2110/jsr.2012.19, 2012.
- 778 van de Schootbrugge, B., Bachan, A., Suan, G., Richoz, S., Payne, J. L.: Microbes, mud, and methane: Cause and  
779 consequence of recurrent Early Jurassic anoxia following the end-Triassic mass-extinction, *Palaeont.*, 56, 685-709,  
780 2013.
- 781 van de Schootbrugge, B., Bailey, T. R., Katz, M. E., Wright, J. D., Rosenthal, Y., Feist-Burkhardt, S., and Falkowski, P. G.:  
782 Early Jurassic climate change and the radiation of organic walled phytoplankton in the Tethys Sea, *Paleobiology*, 31,  
783 73–97, 2005.
- 784 Vasconcelos, C., McKenzie, J. A., Bernasconi, S., Grujic, D., and Tien, A. J.: Microbial mediation as a possible mechanism  
785 for natural dolomite formation at low temperatures, *Nature*, 377, 220–222, 1995.
- 786 Veizer, J., Godderis, Y., and François, L. M.: Evidence for decoupling of atmospheric CO<sub>2</sub> and global climate during the  
787 Phanerozoic eon, *Nature*, 408, 698-701, 2000.
- 788 Wang, Q. W., Liang, B., Kan, Z. Z.: Carbon and oxygen isotopic compositions of lacustrine carbonates of the Early Jurassic  
789 Ziliujing Formation in the Sichuan Basin and their paleolimnological significance, *J. Min. Petr.*, 26(2), 87-91, 2006 (in  
790 Chinese with English abstract).
- 791 Wang, Y. D., Fu, B. H., Xie, X. P., Huang, Q. S., Li, K., Liu, Z. S., Yu, J. X., Pan, Y. H., Tian, N., and Jiang, Z. K.: The  
792 Terrestrial Triassic and Jurassic Systems in the Sichuan Basin, China, in: *Contributions to the 8<sup>th</sup> International Congress  
793 odd the Jurassic System*, edited by: Sha, J. G., Shi, X. Y., Zhou, Z. H., Wang, Y. D., Uni. Sci. Techn., China Press,  
794 Hefei, Anhui, 1-136, 2010 (in Chinese).
- 795 Wang, Y. D., Mosbrugger, V., and Zhang, H.: Early to Middle Jurassic vegetation and climatic events in the Qaidam Basin,  
796 Northwest China, *Palaeogeogr. Palaeoclimatol. Palaeoecol.*, 224, 200–216,

797 <http://dx.doi.org/10.1016/j.palaeo.2005.03.035>, 2005.

798 Warren, J.: Dolomite: occurrence, evolution and economically important associations, *Earth Sci. Rev.*, 52, 1–81, 2000.

799 Wei, M.: Continental Mesozoic Stratigraphy and Paleontology in the Sichuan Basin, People's Publ. House of Sichuan,  
800 Chengdu, 346-363, 1982 (in Chinese with English summary).

801 Wen, W. and Zhao, B.: Stratigraphic character and sedimentary facies of the Ziliujing Formation in the Pujiang-Ya'An area,  
802 Sichuan province, *J. Stratigr.*, 34(2), 219-224, 2010 (in Chinese with English abstract).

803 Wright, V. P.: Paleosol Recognition: A guide to early diagenesis in terrestrial settings (Chapter 12), in: *Developments in*  
804 *Sedimentology*, edited by: Wolf K, H. and Chilingarian, G. V., 47, 591-619, 1992.

805 Xu, W. M., Ruhl, M., Jenkyns, H. C., Leng, M. J., Huggett, J. M., Minisini, D., Ullmann, C. V., Riding, J. B., Weijers, J. W.  
806 H., Storm, M. S., Percival, L. M. E., Tosca, N. J., Idiz, E. F., Tegelaar, E. W., Hesselbo, S. P.: Evolution of the Toarcian  
807 (Early Jurassic) carbon-cycle and global climatic controls on local sedimentary processes (Cardigan Bay Basin, UK),  
808 *Earth Planet. Sci. Lett.*, 484, 396-411, 2018.

809 Xu, W. M., Ruhl, M., Jenkyns, H. C., Hesselbo, S. P., Riding, J. B., Selby, D., Naafs, B. D. A., Weijers, J. W. H., Pancost, R.  
810 D., Tegelaar, E. W., and Idiz, E. F.: Carbon sequestration in an expanded lake system during the Toarcian oceanic  
811 anoxic event, *Nat. Geosci.*, 129-135, doi, 10. 1038/NGEO2871, 2017.

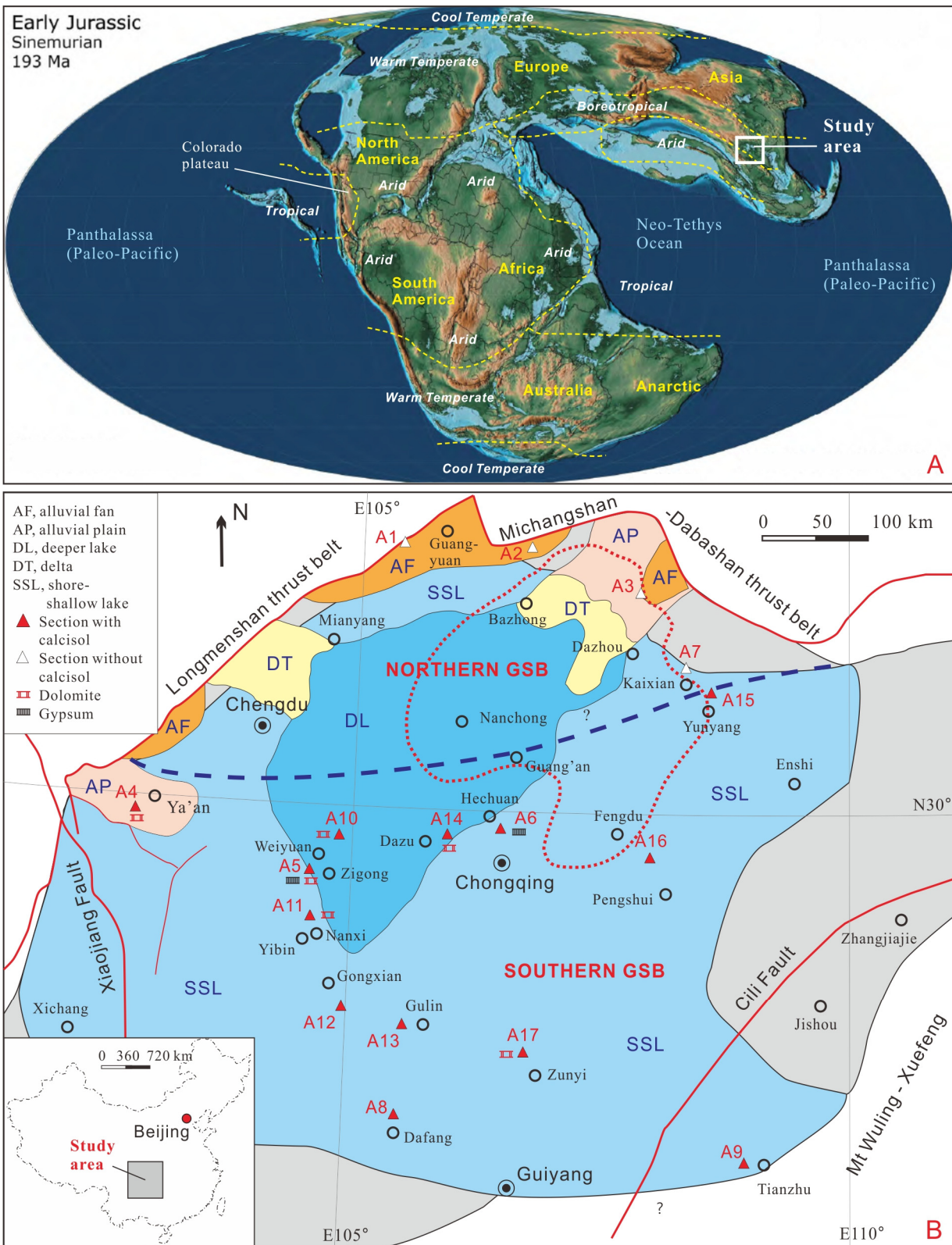
812 Yang, G. L.: Heavy mineral stratigraphy of Mesozoic continental clastic facies in Yaxi area, northern Guizhou, *J. Stratigr.*,  
813 39(1), 89-96 , 2015 (in Chinese with English abstract).

814 Ye, M. N., Liu, X. Y., and Huang, G. Q.: Late Triassic and Early-Middle Jurassic fossil plants from northeastern Sichuan,  
815 *Sci. Techn. Press. Hefei, Anhui*, 1986 (in Chinese with English summary).

816 Zhang, X. S., Zhao, B., Tan, M., Zhou, B. Y., Sun, J.: Stratigraphic Characteristics of Ziliujing Formation, Jurassic Series  
817 and Discovery of Dinosaur Footprints in Dafang, Guizhou, *Geol. Guizhou*, 33(1), 50-70, 2016 (in Chinese with English  
818 abstract).

819 Zhang, Z. L. and Meng, F. S.: Chapter 2, the Jurassic. In Zhang Zhenlai and Meng Fansong eds. *The Triassic-Jurassic*  
820 *Biostratigraphy in Yangtze Gorges (4)*, Geol. Publ. House, Beijing, 408, 1987 (in Chinese with English summary).

821



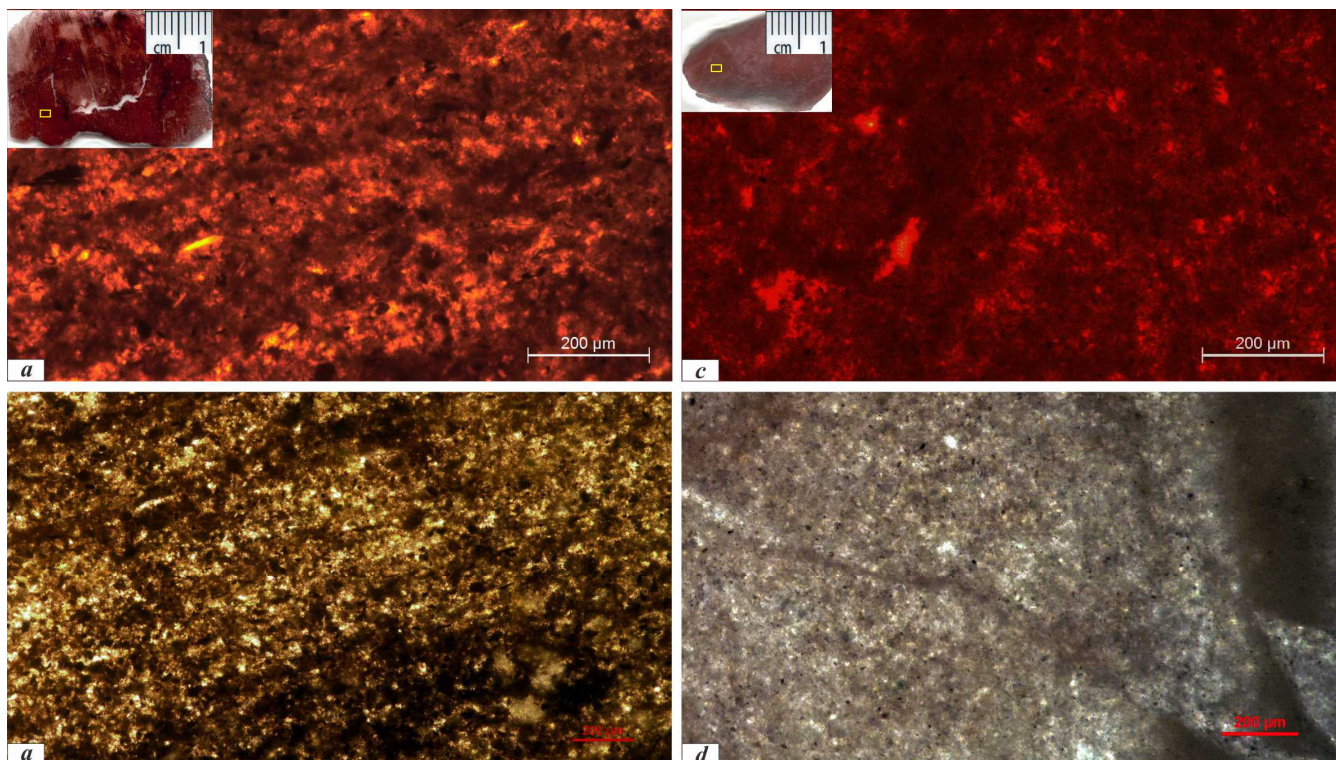
823

824 **Figure 1** A, Global Early-Middle Jurassic climate zones (Boucot et al., 2013) laid on the Early Jurassic (~193 Ma, Sinemurian)  
 825 paleogeographic map (Scotese, 2014). B, Lithofacies paleogeographic sketch of the grand Sichuan paleobasin (GSB) in the early  
 826 Early Jurassic (Zhenzhuchong and Dongyuemiao members) showing locations of the observed and analysed sections and  
 827 climate-sensitive sediments. Lithofacies paleogeographic map was composed and modified from Ma et al. (2009) and Li and He  
 828 (2014). Blue area is the extent of paleolake, estimated as ~380,000 km<sup>2</sup>; blue + gray region is the basin shape, estimated ~480,000  
 829 km<sup>2</sup>. Dot red line confines the deeper lake area in the late Early Jurassic (Ma'anshan and Da'anzhai members). Bold dashed line is

830 the northern edge of calcisol occurrence, which may separate the climate of the GSB as the northern and southern types. Triangles  
831 with numbers are locations of observed and analysed sections: A1, Xiasi section, Jian'ge; A2, Puji section, Wangcang; A3,  
832 Shiguansi section, Wanyuan; A4, Shaping section, Ya'an (bed and thickness from Wen and Zhao, 2010); A6, Tanba and Maliping  
833 section, Hechuan (bed and thickness from Wang et al., 2010); A7, Wenquan section, Kaixian (thickness from Wang et al., 2010).  
834 Location and source data of sections A5 and A8-A17 (climate-sensitive sediments) refer to supplementary data Table S1.

835

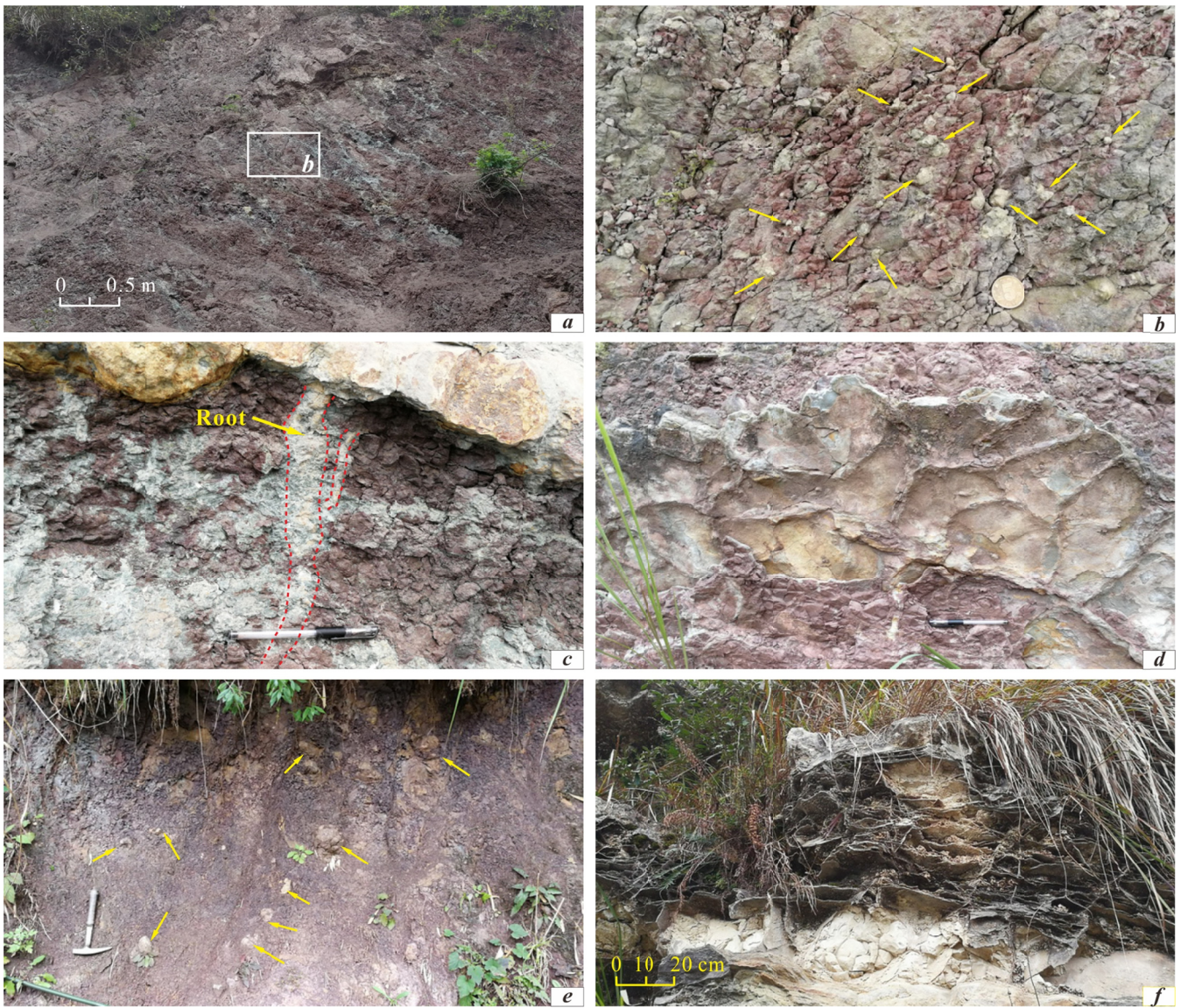
836



837

838 **Figure 2** Microscopic cathodoluminescence photos of representative calcrete samples from the Ziliujing Fm at the Shaping  
839 section, Ya'an. *a*, Sample J<sub>1z</sub>-12-01, Bed B12, Ma'anshan Member; *b*, Sample J<sub>1z</sub>-22-01, Bed B22, Da'anzhai Member. Pedogenic  
840 calcites are mainly null to non-luminescent, minor are orange/red luminescence. Inserts are the scanned photos of thin-section, and  
841 rectangles are the area under cathodoluminescence and drilling.

842



843 **Figure 3** Field photographs of climate-sensitive sediments from the Lower Jurassic Ziliujing Fm in the GSB. *a*, Reddish purple  
 844 calcisol with strong leaching structure. Lower Bed H8 of the upper Ma'anshan Member at Tanba, Hechuan. *b*, Reddish purple  
 845 calcisol showing the density and size of calcretes. The horizon and location same as *a*. Arrows point to calcretes. Coin 2.0 cm  
 846 in diameter. *c*, Reddish purple calcisol with strong leaching structure and rhizoliths. Bed H13 of the top Ma'anshan Member at  
 847 Maliuping, Hechuna. Pen 15 cm long. *d*, Mudcracks. Lower Bed H8 of the upper Ma'anshan Member at Maliuping, Hechuan. Pen  
 848 15 cm long. *e*, Brownish red calcisol with big calcretes (calcareous concretions). Arrows point to big calcretes. Calcisol horizon  
 849 J<sub>1z</sub>-10-01, Bed B10 of Ma'anshan Member at Shaping, Ya'an. Hammer 34 cm long. *f*, Chicken-wire structure. Bed H12 of the  
 850 Da'anzhai Member at Maliuping, Hechuan.

851

852

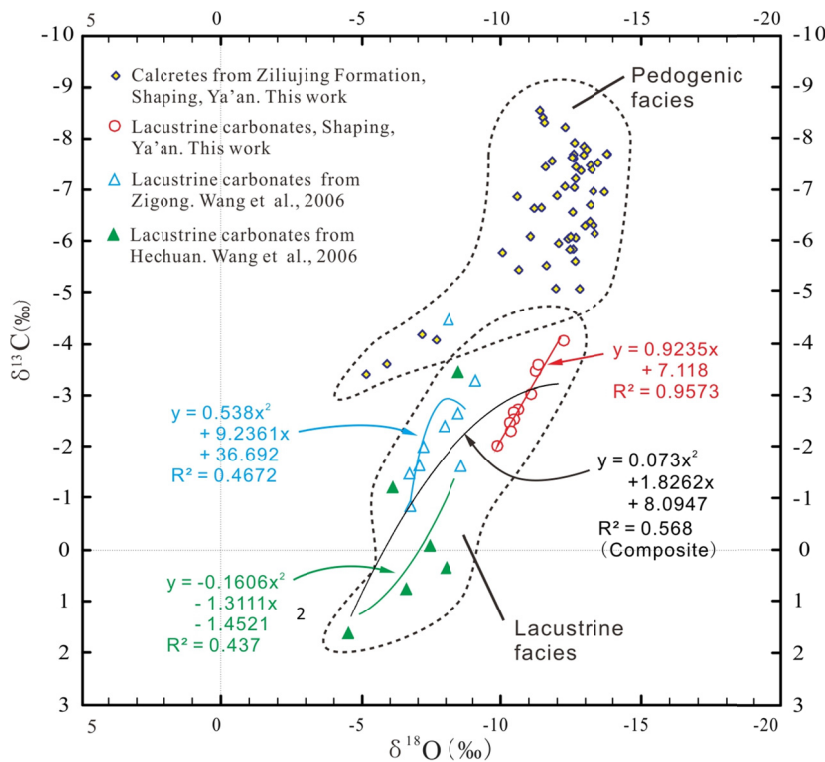
Series	Stage	Fm	Mem	A4	A10	A14	A6	A16	A15	A5	A11	A12	A13	A17	A8	A9	
174																	
(Ma)																	
176	Toa	Ziliujing?	Da'anzhai	West						East							
178																	
180																	
182.7	Pli	Ziliujing?	Ma'anshan														
190.8																	
194	Sin	Ziliujing?	Dongyue-mao														
196																	
198																	
199.3	Het	Ziliujing?	Zhengzhuchong														
201.3																	
				Qijiang		Qijiang						Qijiang					

▭▭▭▭ Hiatus ▲ Calcisol □ Dolomitic sediment ■ Gypsum?

853 **Figure 4** Diagram showing the temporal and spatial variation of climate-sensitive sediments in GSB. Section loactions and data  
854 sources refer to Table S1.

855

856



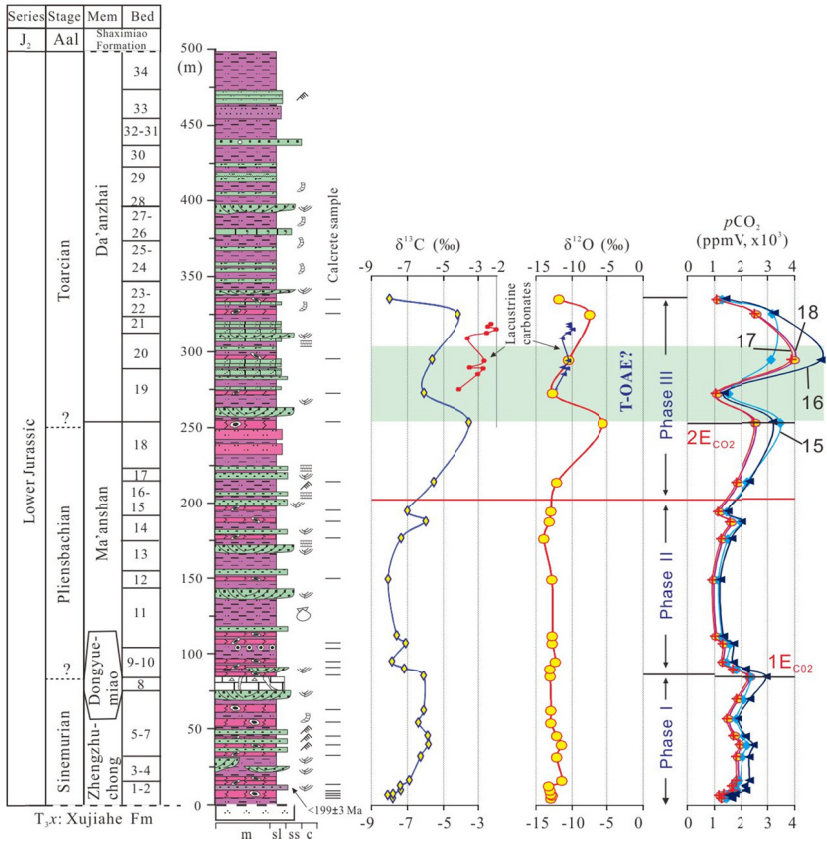
857 **Figure 5** Cross-plot and covariance of carbon and oxygen isotopic values of the Lower Jurassic pedogenic and lacustrine  
858 carbonates from the GSB. Note, the pronounced covariance ( $R^2=0.957$ ) between  $\delta^{13}\text{C}$  and  $\delta^{18}\text{O}$  from Shaping section, Ya'an,  
859 indicating a compositional arid-evaporate and closed pattern lake; the moderate covariance ( $R^2=0.47$  and  $0.44$ ) between  $\delta^{13}\text{C}$  and  
860  $\delta^{18}\text{O}$  from Zigong and Hechuan, indicating a (semi-) arid and semi-closed pattern lake.

861

862

863

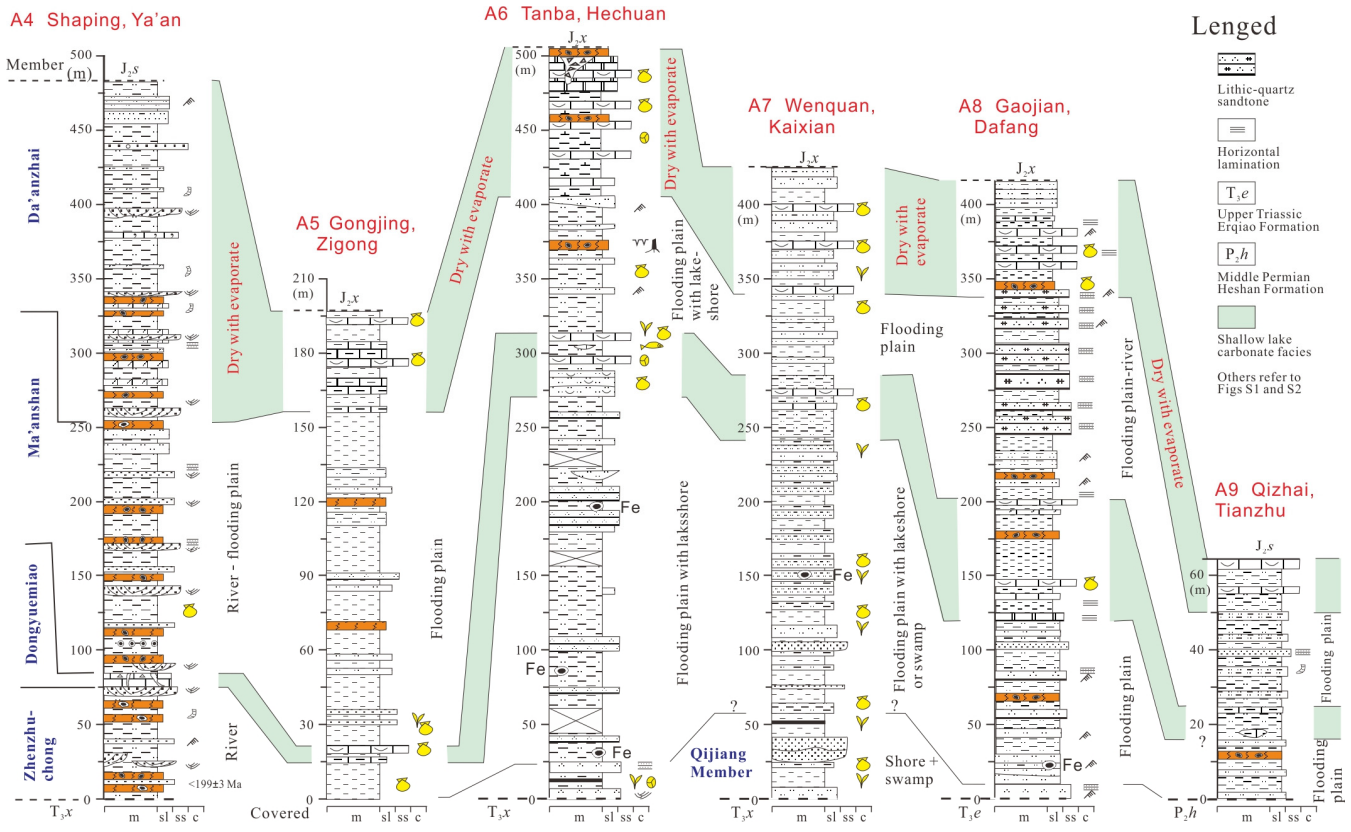




864

865 **Figure 6** Diagram of the Lower Jurassic strata and lithological log at the Shaping section, Ya'an with carbon and oxygen isotope  
 866 values of pedogenic and lacustrine carbonates and  $pCO_2$  cruve. Three phases and two events can be observed for both stable  
 867 isotope values of pedogenic carbonates and  $pCO_2$  estimate. Legend of lithology in log refers to supplementary Figs. S1 and S2.  
 868 T-OAE, Toarcian oceanic anoxic event.  $1E_{CO_2}$  and  $2E_{CO_2}$ , rapid falling event of  $pCO_2$ . Numbers 15 to 18 are the curves of  $pCO_2$  in  
 869 different parameters, and details refer to supplementary Table S4.

870



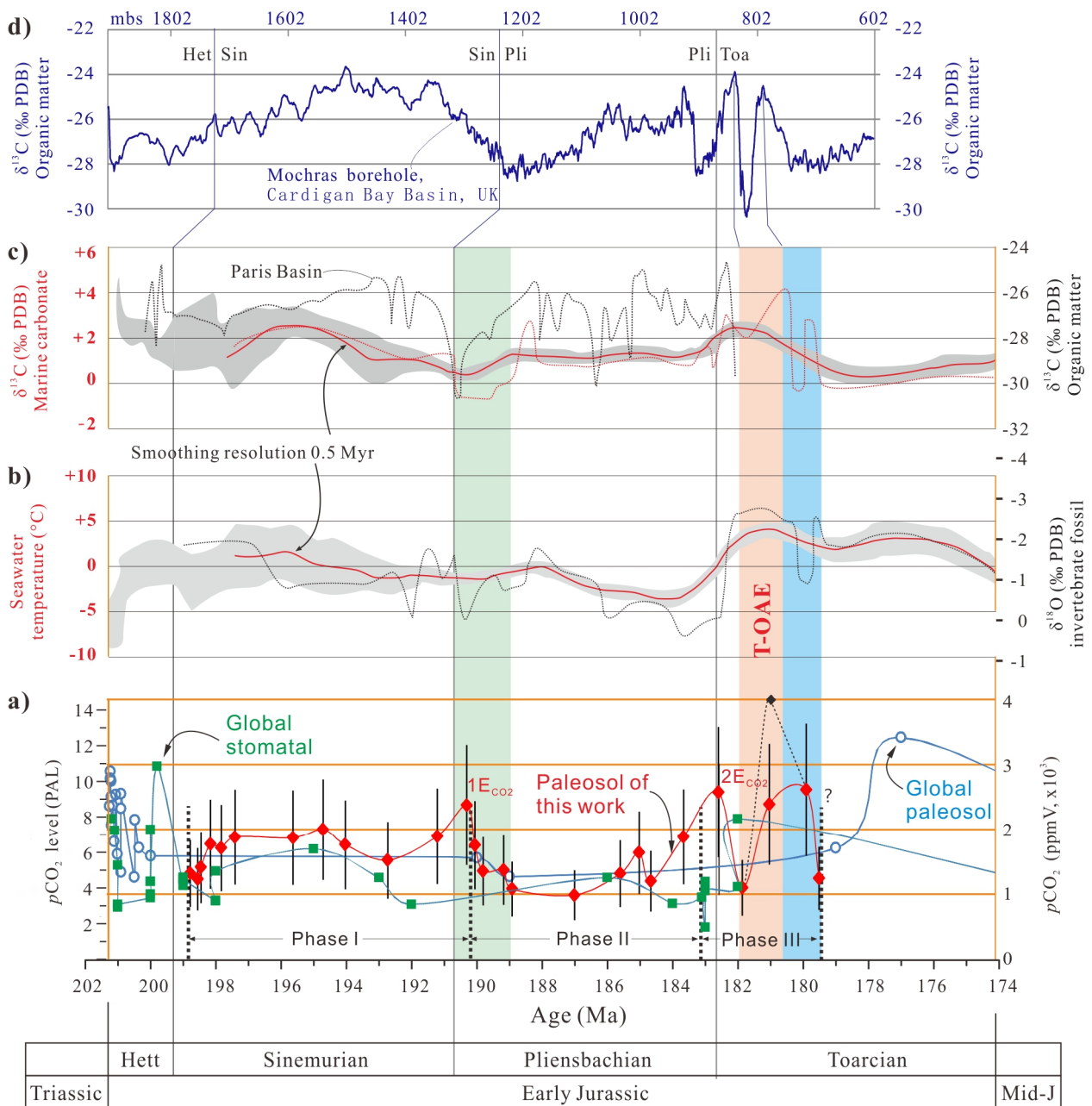
871

872

**Figure 7 Stratigraphic correlation and depositional environment interpretation of the Lower Jurassic in the GSB. Data of**

873

874



875 **Figure 8** Comparison among the Early Jurassic  $p\text{CO}_2$ ,  $\delta^{13}\text{C}$  of marine carbonates and organic matters,  $\delta^{18}\text{O}$  of invertebrate  
876 fossils, and seawater temperature. Age model is from Cohen et al. (2013). a),  $p\text{CO}_2$  values of this work and the composite  $p\text{CO}_2$  by  
877 paleosol and stomatal index (supplementary Table S6 and S7). Vertical bars are errors ( $1\sigma$ ) of  $p\text{CO}_2$  (Table S5). Errors are  
878 propagated using the Gaussian approach (Breecker and Retallack, 2014). Note: 1)  $p\text{CO}_2 = 4027$  ppmV (black solid diamond,  
879 sample J1z-20-01) if the  $\delta^{13}\text{C}_r = -29.0$  ‰ at 181 Ma from Xu et al. (2018) in case of other constant parameters; 2) the early  
880 published  $p\text{CO}_2$  values from both carbon isotope of pedogenic carbonates and stomatal index of fossil plants (data refer to Table  
881 S6 and S7) were awfully rough dated with the average age of a lithostratigraphic formation or group, with which the uncertainty  
882 can be upto 10 Myr, leading to the difficulty of precise and accurate  $p\text{CO}_2$  correlation in pace, frequency, and event. b),  $\delta^{18}\text{O}$  and  
883 seawater temperature (black dot line) of marine invertebrate fossils compiled from Rosales et al. (2001, 2004), Jenkyns et al. (2002),  
884 Bailey et al. (2003), van de Schootbrugge et al. (2005), Gómez et al. (2008), Metodiev and Koleva-Rekalova (2008), Suan et al.  
885 (2008), Korte et al. (2009), Dera et al. (2011), Gómez et al. (2015). c), red dot line  $\delta^{13}\text{C}$  of marine carbonates in western Tethys,  
886 composed from Jenkyns and Clayton (1986, 1997), Hesselbo et al. (2000), Dera et al. (2011), Arabas et al., 2017; black dot and solid  
887 line  $\delta^{13}\text{C}$  of organic matters from Paris Basin, France (Peti et al., 2017). Smoothed  $\delta^{18}\text{O}$  and seawater temperature (red curves) in  
888 b) and c) are after Dera et al. (2011). d),  $\delta^{13}\text{C}$  of organic matters from North Atlantic. Composed from the Mochras borehole,  
889 Cardigan Bay Basin, UK (Xu et al., 2018; Storm et al., 2020), seven-point average smoothing against depth (mbs).

890

892 **Table 1 Stratigraphic framework of the Lower Jurassic Ziliujing Fm in Sichuan and adjacent area (GSB), Southwest China**

Epoch	Age	Formation	W Sichuan (Ya'an)	E Sichuan and Chongqing	S Sichuan and N Guizhou	N Sichuan
Middle Jurassic	Aalenian	Xintiangou Fm	Xintiangou Fm	Xintiangou Fm	Xintiangou Fm	Qianfuyan / Xintiangou Fm
Early Jurassic	Toarcian	Ziliujing Fm	Da'anzhai Mem (Bed 20-34)	Da'anzhai Mem	Da'anzhai Mem	Baitianba Fm
	Pliensbachian		Ma'anshan Mem (Bed 9-18)	Ma'anshan Mem	Ma'anshan Mem	
	Sinemurian		Dongyuemiao Mem (Bed 8)	Dongyuemiao Mem	Dongyuemiao Mem	
			Zhenzhuchong Mem (Bed 1-7)	Zhenzhuchong Mem	Zhenzhuchong Mem	
	Hettangian		<b>Hiatus</b>	Qijiang Mem	Qijiang Mem	
Late Triassic	Rhaetian	Xujiahe Fm	Xujiahe Fm	Xujiahe Fm	Xujiahe Fm	

Notes: Straigraphic classification and correlation were composed from Dong (1984); SBGM (1997), Wang et al. (2010), Wen and Zhao (2010), Xu et al (2017). Re-Os isotope age of the lower Da'anzhai Member is  $180.3 \pm 3.2$  Ma in western Sichuan (Xu et al., 2017). Fm, Formation; Mem, Member.

893

894 **Supplementary data**895 **Captions of supplementary figures**

896 **Figure S1 Lithological log of the Lower Jurassic Ziliujing Fm with depositional environment interpretations and sample**  
897 **positions at the Shaping section, Ya'an of Sichuan. Bed number and thickness are partly referred to Wen and Zhao (2010).**

898

899 **Figure S2 Lithological log of the Lower Jurassic Ziliujing Fm at the Tanba-Maliuping section, Hechuan of Chongqing with**  
900 **depositional environment interpretations and sample positions. Bed number and thickness are partly referred to Wang et al**  
901 **(2010).**

902

903 **Figure S3 Field photographs of the Lower Jurassic Ziliujing Fm lithofacies in the GSB. a, Well roundness and sorting gravels in**  
904 **the alluvial fan conglomerate. Basal and lower Baitianba Fm. Puji, Wangcang. Hammer 30 cm long. b, Large trough**  
905 **cross-bedding with scours in the point bar and channel sandstones. Upper Baitianba Fm; Puji, Wangcang. c, Calcisol developed**  
906 **within strong leaching overbank mudrocks on channelized sandstones. Middle of Bed B2, the Zhenzhuchong Member, Shaping**  
907 **section, Ya'an. d, Purple red mudrocks intercalated with thin siltstones in flood plain facies. Bed H7 of the Ma'anshan Member,**  
908 **Tanba section, Hechuan. e, Whitish medium-thick micritic dolomites in lacustrine facies. Bed H12 of the Da'anzhai Member,**  
909 **Maliuping section, Hechuan. Hammer 34 cm long. f, Greeinsh gray lacustrine muddy dolomites and dolomitic mudrocks**  
910 **associated with brownish / reddish purple mudrocks. Bed B21 of the Da'anzhai Member, Shaping section, Ya'an.**

911

912 **Figure S4 Microscopic photos showing lithological microfacies of the Lower Jurassic Ziliujing Fm. a, Fine lithic (quartz)**  
913 **sandstone. Lithic-dominant fragments are mudrock. Sample J<sub>1z</sub>-02-01b, Zhenzhuchong Member, Shaping section, Ya'an.**  
914 **Plain-polarised light. b, Laminated muddy dolomite and dolomitic mudrocks. Sample J<sub>1z</sub>-21S2B, Da'anzhai Member, Shaping**  
915 **section, Ya'an. Plain-polarised light. c, Fine quartz arenite. Sample 18HC-02b3, Bed H2, Qijiang Member, Tanba section,**  
916 **Hechuan. Cross-polarised light. d, Micritic dolomite. Sample 18HC-06b, Bed H12, Da'anzhai Member, Maliuping section,**  
917 **Hechuan. Plain-polarised light. e, Coquina. Shell wall of bivalves were micritized. Mud and recrystalline calcites filled inter-shells**

918 and intra-shells. Sample 18HC-04b, Base of Bed H12, Da'anzhai Member, Maliuping section, Hechuan. Cross-polarised light. *f*,  
919 Relict of coquina. Shell wall of bivalves were partly micritized. Strongly recrystalline calcites replaced the fills and shells. Sample  
920 18HC-05b, Bed H12, Da'anzhai Member, Maliuping section, Hechuan. Cross-polarised light.

921  
922 **Figure S5** Field photographs of the Lower Jurassic Ziliujing Fm lithofacies in the GSB. *a*, Lithofacies and stratigraphic sequence.  
923 Beds B8 to B10 of the lower Ma'anshan and Dongyuemiao members at Shaping, Ya'an. *b*, Karstified gravels within the limestone.  
924 The horizon and location is same as *a*. Pen 15 cm long. *c*, Layered dolomites with Karstified cave gravels. Bed H12 of the  
925 Da'anzhai Member at Maliuping, Hechuan. *d*, Karstified cave gravels. The horizon and location is same as *c*. Hammer 34 cm long.

926  
927 **Figure S6** Stratigraphic correlation of the Lower Jurassic Baitianba Fm in northern GSB. Locations and sources refer to Figure  
928 1. Plant fossils and stratal thickness in the Shiguansi section, Wanyuan are cited from SBG (1980b).

929

### 930 Captions of supplementary tables

931 **Table S1** Occurrence list of the Early Jurassic climate-sensitive sediments in the GSB

932

933 **Table S2** Early Jurassic paleosols in Ya'an of Sichuan and Hechuan of Chongqing, Southwest China

934

935 **Table S3** Carbon-oxygen isotope composition of lacustrine carbonates from the Lower Jurassic Ziliujing Fm (Da'anzhai Mem) in  
936 the GSB

937

938 **Table S4**  $p\text{CO}_2$  estimate by carbon isotope of pedogenic carbonates from the Lower Jurassic Ziliujing Fm at Shaping, Ya'an  
939 of Sichuan

940

941 **Table S5** Calculation of  $p\text{CO}_2$  and Gaussian error propagation using the atmosphere determination of global organic matter  
942 isotope composition for the Early Jurassic Sichuan paleobasin

943

944 **Table S6** Global  $p\text{CO}_2$  data of the Latest Triassic - Early Jurassic by stomatal method

945

946 **Table S7** Global  $p\text{CO}_2$  data of the Latest Triassic - Early Jurassic estimated by carbon isotope of pedogenic carbonates

947

948 **Table S8** Calculation of  $p\text{CO}_2$  and Gaussian error propagation using the atmosphere carbon isotope determination of marine  
949 fossil carbonate carbon isotope composition for the Early Jurassic Sichuan paleobasin

### 950 Captions of supplementary notes

951 **Note S1**, Description and interpretation of sedimentary facies and its evolution

952

953